

Penalized Projected Kernel Calibration for Computer Models*

Yan Wang †

Abstract. Projected kernel calibration is known to be theoretically superior, its loss function is abbreviated as PK loss function. In this work, we prove the uniform convergence of PK loss function and show that (1) when the sample size is large, any local minimum point and local maximum point of the L_2 loss between the true process and the computer models is a local minimum point of the PK loss function; (2) all the local minimum values of the PK loss function converge to the same value. These theoretical results imply that it is extremely hard for the projected kernel calibration to identify the global minimum point of the L_2 loss which is defined as the optimal value of the calibration parameters. To solve this problem, a frequentist method, called the penalized projected kernel calibration method is proposed. As a frequentist method, the proposed method is proved to be semi-parametric efficient. On the other hand, the proposed method has a natural bayesian version, which allows users to calculate the credible region of the calibration parameters without using a large sample approximation. Through extensive simulation studies and a real-world case study, we show that the proposed calibration can accurately estimate the calibration parameters, and compare favorably to alternative calibration methods regardless of the sample size.

Key words. Projected kernels, Calibration of computer models, Stationary points, Penalized projected kernel calibration

AMS subject classifications. 62G08, 62M30, 62M40

1. Introduction. Computer models or simulators are increasingly used to reproduce the behavior of complex systems in physics, engineering and human processes. Computer models usually involve model parameters that cannot be determined or observed in the physical processes. The input values of these model parameters can significantly affect the accuracy and usefulness of the computer outputs. When physical observations are available, one can adjust the computer model parameters so that the computer outputs match the physical data. This activity is called the *calibration* of computer models and these model parameters are called *calibration parameters*.

The celebrated bayesian calibration method by Kennedy and O'Hagan [6] is one of the major and widely used approaches for the calibration of computer models. We refer to [6] to give more details about computer model calibration. Assume the set of design points for the physical experiments is $\mathbf{X} = \{\mathbf{x}_1, \dots, \mathbf{x}_n\}$, where $\mathbf{x} = (x_1, \dots, x_d)^T \in \Omega \subset \mathbf{R}^d$ and the set of corresponding physical observations is $\mathbf{Y} = (y_1, \dots, y_n)^T$. The boldface notation will be used for matrices and vectors whose size depends on n and the superscript T represents transpose. Suppose the physical experimental observation is generated by

$$(1.1) \quad y_i = \zeta(\mathbf{x}_i) + \epsilon_i,$$

where $i = 1, \dots, n$. $\zeta(\cdot)$ is called the *true process*, which is an unknown function, and ϵ_i 's are

*Submitted to the editors DATE.

Funding:

†School of Statistics and Data Science, Faculty of Science, Beijing University of Technology, Beijing 100124, China (yanwang@bjut.edu.cn).

the observation errors following $N(0, \sigma^2)$ with unknown $\sigma^2 < \infty$.

Denote $\boldsymbol{\theta} = (\theta_1, \dots, \theta_q)^T \in \Theta \subset \mathbf{R}^q$ as the set of calibration parameters and $y^s(\mathbf{x}, \boldsymbol{\theta})$ the computer model. The idea of calibration is to find the values of the calibration parameters so that the computer outputs are close to the physical experimental observations. Kennedy and O'Hagan (abbreviated as KO thereafter) claim that, as the computer models are usually built under assumptions and simplifications which are not exactly correct in reality, the computer outputs cannot perfectly fit the physical experimental observations. That is, there is *model discrepancy* between the true process and the computer model. KO use the following model (named as KO's model) to take this model discrepancy into account:

$$(1.2) \quad \zeta(\cdot) = y^s(\cdot, \boldsymbol{\theta}^*) + \delta(\cdot),$$

where $\boldsymbol{\theta}^*$ denotes the combination of the optimal calibration parameters and δ is the *model discrepancy function*. The goal of calibration is to estimate $\boldsymbol{\theta}^*$. However, equation (1.2) is not enough to fully determine $\boldsymbol{\theta}^*$, because the function δ is also unknown.

By assuming that the model discrepancy function is one realization of a Gaussian Process, KO give a bayesian estimator of the calibration parameter. Tuo and Wu [19] show that the estimator given by KO can't converge to $\boldsymbol{\theta}^*$, and the optimal calibration parameters $\boldsymbol{\theta}^*$ is defined as

$$(1.3) \quad \boldsymbol{\theta}^* := \underset{\Theta}{\operatorname{argmin}} L_2(\boldsymbol{\theta}),$$

where

$$(1.4) \quad L_2(\boldsymbol{\theta}) = \int_{\Omega} (\zeta(\mathbf{x}) - y^s(\mathbf{x}, \boldsymbol{\theta}))^2 d\mathbf{x}$$

is the L_2 loss between the true process and the computer model.

Much efforts have been made to obtain a consistent estimator of the calibration parameter. Tuo and Wu [19] plug the kernel ridge regression of ζ into (1.3) to get the L_2 estimator. Wong et al. [25] propose a least square estimator. Gu and Wang [3] point out that both the two approaches have limitations in calibration and prediction, especially when the number of physical observations is small. To predict the true process model more accurate, Gu and Wang [3] propose a scaled Gaussian Process model to mimic the model discrepancy function and give a new bayesian calibration method based on KO's model, named as scaled Gaussian Process model calibration method. The convergence rate of estimator given by scaled Gaussian Process model calibration method is proven to be slower than $n^{-1/2}$ [4] in contrast to the L_2 calibration and least square calibration. This slower convergence rate may not be desired when an efficient estimator of the calibration parameter is needed. To estimate the calibration parameter well, by adding an orthogonality constraint (2.4) to KO's model, Tuo [17] suggests a projected kernel calibration method and proves the semi-parametric consistency of this estimator. The projected kernel calibration has been applied to the calibration of the composite fuselage simulation successfully with small sample size [23]. However, a numerical simulation in [3] shows that the projected kernel calibration may get stuck in local minimum or even local maximum of the L_2 loss, especially when the sample size is large.

In this work, we first verify the simulation results in [3] theoretically and then proposed a new calibration method which is more robust with respect to changing the number of physical observations. The contributions of this work include two aspects:

Firstly, the performance of the projected kernel calibration is explored and the results have:

- Any local minimum point and local maximum point of the L_2 loss function is a local minimum point of the projected kernel loss function (3.3);
- All the local minimum values of the projected kernel loss function converge to the same value as the sample size tends to infinity.
- The projected kernel loss function uniformly converges to a projected kernel L_2 loss function (3.14);

These results imply that, it is extremely hard for the projected kernel calibration to identify the global minimum point of the L_2 loss function.

Secondly, to address the problem that the projected kernel calibration faced with, a penalized projected kernel calibration method is proposed. The main idea is to add a penalty $\|\delta\|_{L_2(\Omega)}$ to the projected kernel loss function, such that any local maximum point of the L_2 loss function will not be a local minimum point of the proposed loss function, and the local minimum values of the proposed loss function are different with each other even for a sufficiently large n . The proposed method is proven to be semi-efficient. Theoretical comparison between the proposed method and some existing calibration methods is shown in Table 1.

Table 1
Comparison of different calibration methods

Method	Abbreviation	Consistence (Y/N)	Penalty	Consistence rate (n^{-t})
KO's calibration [6]	KO	N	$\ \delta\ _{\mathcal{N}_K(\Omega)}$	$m/(4m+d)^{(1)}$
L_2 calibration [19]	L_2	Y	$\ \delta\ _{\mathcal{N}_K(\Omega)}$	1/2
Least square calibration [25]	LS	Y	$\ \delta\ _{\mathcal{N}_K(\Omega)}$	1/2
Scaled Gaussian Process model calibration [3]	SGP	Y	$\ \delta\ _{\mathcal{N}_K(\Omega)}$ and $\ \delta\ _{L_2(\Omega)}$	$m/(2m+d)$
Projected kernel calibration [17]	PK	Y	$\ \delta\ _{\mathcal{N}_{K_\theta}(\Omega)}$	1/2
Penalized projected kernel calibration	PPK	Y	$\ \delta\ _{\mathcal{N}_{K_\theta}(\Omega)}$ and $\ \delta\ _{L_2(\Omega)}$	1/2

Remark 1: Under certain conditions, $\hat{\theta}_{KO}$ converges to $\arg\min_{\Theta} \|\delta\|_{\mathcal{N}_K(\Omega)}$ with the convergence rate $O_p(n^{-\frac{m}{4m+d}})$, see [18].

The remainder of this paper is organized as follows. In Section 2, we give a brief review of the projected kernel calibration. In Section 3, the performance of the projected kernel calibration method are examined theoretically and a simulated example is conducted to verify these theoretical assertions. In Section 4, a penalized projected kernel calibration method and its convergence properties are given. Computation problems are addressed in Section 5. Two numerical simulation studies and a spot welding study are conducted in Section 6. Concluding remarks and further discussions are given in Section 7.

2. Review on projected kernel calibration. In this section we review the projected kernels and the projected kernel calibration.

2.1. Projected kernels. Let $K(\cdot, \cdot)$ to be a positive definite kernel function over $\Omega \times \Omega$, such as the Matérn kernel function [11, 14] with

$$(2.1) \quad K(h; \nu, \rho) = \frac{1}{\Gamma(\nu)2^{\nu-1}} \left(\frac{h}{\rho}\right)^\nu K_\nu\left(\frac{h}{\rho}\right), \nu > 0, \rho > 0,$$

where $h = \|\mathbf{x}_i - \mathbf{x}_j\|$; K_ν is the modified Bessel function of the second kind; ν and ρ are fixed parameters. Suppose \mathcal{G} is a finite-dimensional subspace of $L_2(\Omega)$ with $\dim \mathcal{G} = q$ and $\{e_1, \dots, e_q\}$ is a set of orthonormal basis of \mathcal{G} . For any $f \in L_2(\Omega)$, let $\mathcal{P}_{\mathcal{G}}f := \sum_{i=1}^q \langle f, e_i \rangle e_i$ be the projection of f onto \mathcal{G} and $\mathcal{P}_{\mathcal{G}}^\perp f = f - \mathcal{P}_{\mathcal{G}}f$ be the perpendicular component. Then the projected kernel of K is defined as

$$(2.2) \quad K_{\mathcal{G}} = K - \mathcal{P}_{\mathcal{G}}^{(1)}K - \mathcal{P}_{\mathcal{G}}^{(2)}K + \mathcal{P}_{\mathcal{G}}^{(1)}\mathcal{P}_{\mathcal{G}}^{(2)}K,$$

where $\mathcal{P}_{\mathcal{G}}^{(1)}, \mathcal{P}_{\mathcal{G}}^{(2)}$ are projection transformations from $L_2(\Omega \times \Omega)$ to $L_2(\Omega \times \Omega)$,

$$(2.3) \quad \begin{aligned} \mathcal{P}_{\mathcal{G}}^{(1)}K(\mathbf{x}_1, \mathbf{x}_2) &= \sum_{j=1}^q e_j(\mathbf{x}_1) \int_{\Omega} K(\mathbf{x}, \mathbf{x}_2) e_j(\mathbf{x}) d\mathbf{x}, \\ \mathcal{P}_{\mathcal{G}}^{(2)}K(\mathbf{x}_1, \mathbf{x}_2) &= \sum_{j=1}^q e_j(\mathbf{x}_2) \int_{\Omega} K(\mathbf{x}_1, \mathbf{x}) e_j(\mathbf{x}) d\mathbf{x}, \\ \mathcal{P}_{\mathcal{G}}^{(1)}\mathcal{P}_{\mathcal{G}}^{(2)}K(\mathbf{x}_1, \mathbf{x}_2) &= \sum_{j=1}^q e_j(\mathbf{x}_1) e_j(\mathbf{x}_2) \int_{\Omega} \int_{\Omega} K(\mathbf{x}, \mathbf{t}) e_j(\mathbf{t}) e_j(\mathbf{x}) d\mathbf{t} d\mathbf{x}. \end{aligned}$$

Theorem 3.2 in [17] proves the positive definiteness of $K_{\mathcal{G}}$.

2.2. Projected kernel calibration. Because (1.3) is generally equivalent to the orthogonality constraints

$$(2.4) \quad \int_{\Omega} \frac{\partial y^s(\mathbf{x}, \boldsymbol{\theta}^*)}{\partial \theta_j} \delta(\mathbf{x}) d\mathbf{x} = 0,$$

for $j = 1, 2, \dots, q$. Tuo [17] claims that the function space that $\delta(\cdot)$ belongs to should be orthogonal to $\mathcal{G}_{\theta} = \text{span}\{\frac{\partial y^s(\cdot, \theta)}{\partial \theta_2}, \frac{\partial y^s(\cdot, \theta)}{\partial \theta_1}, \dots, \frac{\partial y^s(\cdot, \theta)}{\partial \theta_q}\}$. Let $K_{\theta} = K_{\mathcal{G}_{\theta}}$ to be the projected kernel and $\mathcal{N}_{K_{\theta}}(\Omega)$ the reproduced kernel Hilbert Space generated by K_{θ} [24]. By assuming $\delta(\cdot) \in \mathcal{N}_{K_{\theta}^*}(\Omega)$, the projected kernel smoothing estimator $(\hat{\boldsymbol{\theta}}_{PK}, \hat{\delta}_{PK})$ is defined as the minimizer of

$$(2.5) \quad \frac{1}{n} \sum_{i=1}^n (y_i - \delta(\mathbf{x}_i) - y^s(\mathbf{x}_i, \boldsymbol{\theta}))^2 + \lambda \|\delta\|_{\mathcal{N}_{K_{\theta}}(\Omega)}^2,$$

where λ is a tuning parameter, which can be chosen by generalized cross validation (GCV); see [5].

Following from the representer's theorem [12, 22], $\hat{\boldsymbol{\theta}}_{PK}$ can also be represented by

$$(2.6) \quad \hat{\boldsymbol{\theta}}_{PK} = \underset{\Theta}{\operatorname{argmin}} (\mathbf{Y} - \mathbf{Y}_{\theta}^s)^T (\mathbf{K}_{\theta} + n\lambda \mathbf{I}_n)^{-1} (\mathbf{Y} - \mathbf{Y}_{\theta}^s).$$

where \mathbf{I}_n is a $n \times n$ identity matrix, $\mathbf{Y}_{\theta}^s = (y^s(\mathbf{x}_1, \boldsymbol{\theta}), \dots, y^s(\mathbf{x}_n, \boldsymbol{\theta}))^T$, and $\mathbf{K}_{\theta} = [K_{\theta}(\mathbf{x}_i, \mathbf{x}_j)]_{1 \leq i, j \leq n}$. Theorem 4.3 of [17] shows that the projected kernel estimation $\hat{\boldsymbol{\theta}}_{PK}$ is asymptotically normally distributed and there does not exist a regular estimator with even smaller asymptotic variance than $\hat{\boldsymbol{\theta}}_{PK}$.

A bayesian interpretation for the projected kernel calibration is also given in [17]. Suppose $\zeta(\cdot) - y^s(\cdot, \boldsymbol{\theta})$ is a realization of Gaussian Process $GP(0, \tau^2 K_\theta)$, where τ^2 is the variance of the covariance function and K_θ is the correlation function. Denote the prior distribution of $\boldsymbol{\theta}$ as $\pi(\boldsymbol{\theta})$, the posterior of $\boldsymbol{\theta}$ can be presented as

$$(2.7) \quad \pi(\boldsymbol{\theta} | \mathbf{Y}, \mathbf{Y}^s) \propto \pi(\boldsymbol{\theta}) \times \exp \left\{ -\frac{1}{2} (\mathbf{Y} - \mathbf{Y}_\theta^s)^T (\mathbf{K}_\theta + n\lambda \mathbf{I}_n)^{-1} (\mathbf{Y} - \mathbf{Y}_\theta^s) \right\},$$

where $n\lambda = \sigma^2/\tau^2$ and an uninformative prior is used in projected kernel calibration, that is $\pi(\boldsymbol{\theta}) = 1$.

3. Performance of the projected kernel calibration. We exam the performance of the projected kernel calibration in this section. In subsection 3.1, we redefine the PK loss function, and discuss the relationship between local optima of the L_2 loss function and these of the PK loss function. The uniform convergence of the PK loss function is provided in subsection 3.2, which suggests that the local minimal values of the PK loss function converge to the same value. In subsection 3.3, the numerical study in [3] is revisited to validate our theoretical assertions.

3.1. Local minima of the PK loss function. To find the local minima of PK loss function, it is a natural choice to calculate the first and the second derivatives of the PK loss function: the first derivative at any local minimal point is zero and the Hessian matrix is positive definite. Because the loss function (2.5) depends on $\boldsymbol{\theta}$ and δ , to obtain the derivative of PK loss function, we firstly rewrite (2.5) such that the loss function just depends on $\boldsymbol{\theta}$.

Theorem 3.1. Define $\delta^\theta(\cdot) = \zeta(\cdot) - y^s(\cdot, \boldsymbol{\theta})$, $\delta_i^\theta = y_i - y^s(\mathbf{x}_i, \boldsymbol{\theta})$. Defined the kernel ridge estimator of δ^θ as

$$(3.1) \quad \hat{\delta}_{PK}^\theta(\mathbf{x}) = K_\theta^T(\mathbf{x}, \mathbf{X})(\mathbf{K}_\theta + n\lambda \mathbf{I}_n)^{-1}(\mathbf{Y} - \mathbf{Y}_\theta^s),$$

where $K_\theta(\mathbf{x}, \mathbf{X}) = (K_\theta(\mathbf{x}, \mathbf{x}_1), \dots, K_\theta(\mathbf{x}, \mathbf{x}_n))^T$. Then $\hat{\boldsymbol{\theta}}_{PK}$ can be represented by

$$(3.2) \quad \hat{\boldsymbol{\theta}}_{PK} = \underset{\Theta}{\operatorname{argmin}} L_{PK}(\boldsymbol{\theta}),$$

where

$$(3.3) \quad L_{PK}(\boldsymbol{\theta}) = \frac{1}{n} \sum_{i=1}^n \left(\delta_i^\theta - \hat{\delta}_{PK}^\theta(\mathbf{x}_i) \right)^2 + \lambda \|\hat{\delta}_{PK}^\theta\|_{\mathcal{N}_{K_\theta}(\Omega)}^2.$$

The loss function (3.3) is named as the projected kernel loss function (abbreviated as PK loss function).

By the definition of kernel ridge regression, assume $\mathcal{N}_{K_\theta}(\Omega) \subset \mathcal{N}_K(\Omega)$, we have that $\hat{\delta}_{PK}^\theta$ (3.1) is the minimizer of the loss function l_θ which is defined as

$$(3.4) \quad l_\theta(g_0) = \frac{1}{n} \sum_{i=1}^n \left(\delta_i^\theta - \mathcal{P}_{G_\theta}^\perp g_0(\mathbf{x}_i) \right)^2 + \lambda \|\mathcal{P}_{G_\theta}^\perp g_0\|_{\mathcal{N}_{K_\theta}(\Omega)}^2,$$

where $g_0 \in \mathcal{N}_K(\Omega)$. Suppose $\hat{g}_0 = \operatorname{argmin}_{g_0 \in \mathcal{N}_K(\Omega)} l_\theta(g_0) = \hat{\zeta} - y^s(\cdot, \boldsymbol{\theta}) = \hat{\delta}^\theta$, where $\hat{\zeta}$ is an estimator of ζ , then $\hat{\delta}_{PK}^\theta = \mathcal{P}_{G_\theta}^\perp \hat{\delta}^\theta = \hat{\delta}^\theta - \mathcal{P}_{G_\theta} \hat{\delta}^\theta$.

Theorem 3.2. Define the empirical norm of $f \in \mathcal{N}_{K_\theta}(\Omega)$ as $\|f\|_n = \frac{1}{n} \sum_{i=1}^n f^2(\mathbf{x}_i)$. Then under the following conditions:

- A1. x_i 's are independent random samples from the uniform distribution over Ω .
A2. e_i 's are sub-gaussian, that is, there exists $C > 0$, such that

$$E[\exp(C|e_i|)] < \infty, i = 1, \dots, n.$$

- A3. $\mathcal{N}_K(\Omega)$ can be continuously embedded into the Sobolev space $H^m(\Omega)$ with $m > d/2$.
A4. Assume that

$$\sup_{\boldsymbol{\theta} \in \Theta, j=1,2,\dots,q} \left\{ \left\| \frac{\partial y^s(\cdot, \boldsymbol{\theta})}{\partial \theta_j} \right\|_{\mathcal{N}_K(\Omega)} / \left\| \frac{\partial y^s(\cdot, \boldsymbol{\theta})}{\partial \theta_j} \right\|_{L_2(\Omega)} \right\} < \infty,$$

$$\sup_{\boldsymbol{\theta} \in \Theta, j=1,2,\dots,q} \left\{ \left\| \frac{\partial y^s(\cdot, \boldsymbol{\theta})}{\partial \theta_j} \right\|_{L_2(\Omega)} \right\} < \infty,$$

and

$$\sup_{\boldsymbol{\theta} \in \Theta} \|y^s(\cdot, \boldsymbol{\theta})\|_{\mathcal{N}_K(\Omega)} < \infty.$$

- A5. Define matrix

$$(3.5) \quad \mathbf{E}_\theta = \left[\int \frac{\partial y^s(\mathbf{x}, \boldsymbol{\theta})}{\partial \theta_i} \frac{\partial y^s(\mathbf{x}, \boldsymbol{\theta})}{\partial \theta_j} d\mathbf{x} \right]_{1 \leq i, j \leq q}.$$

Let $\lambda_{\min}(\mathbf{E}_\theta)$ be the minimum eigenvalue of \mathbf{E}_θ , suppose

$$\inf_{\boldsymbol{\theta} \in \Theta} \lambda_{\min}(\mathbf{E}_\theta) > 0.$$

We have that if $\lambda \sim n^{-\frac{2m}{2m+d}}$,

$$(3.6) \quad \sup_{\boldsymbol{\theta} \in \Theta} \|\delta^\theta - \hat{\delta}_{PK}^\theta\|_n = O_p(n^{-\frac{m}{2m+d}}),$$

$$\sup_{\boldsymbol{\theta} \in \Theta} \|\delta^\theta - \hat{\delta}_{PK}^\theta\|_{\mathcal{N}_{K_\theta}(\Omega)} = O_p(1).$$

Invoking the condition that x_i 's follow the uniform distribution over Ω , we apply Lemma 5.16 of [21] to conclude an asymptotic equivalence relation between the L_2 and the empirical norm as:

$$(3.7) \quad \lim_{n \rightarrow \infty} \sup P \left\{ \sup_{\|f\|_{\mathcal{N}_{K_\theta}(\Omega)} = O_p(1), \|f\|_{L_2(\Omega)} > \tau n^{-\frac{m}{2m+d}}/\eta} \left| \frac{\|f\|_n}{\|f\|_{L_2(\Omega)}} - 1 \right| \geq \eta \right\} = 0.$$

That is, we have

$$(3.8) \quad \sup_{\boldsymbol{\theta} \in \Theta} \|\delta^\theta - \hat{\delta}_{PK}^\theta\|_{L_2(\Omega)} = O_p(n^{-\frac{m}{2m+d}}).$$

Remark 3.3. Condition (A3) can be met easily if K is chosen to be a Matérn kernel. By the Corollary 1 of [20], the reproduced kernel Hilbert space generated by the Matérn kernel $K(d; \nu, \rho)$ is equal to the (fractional) Sobolev space $H^{\nu+d/2}(\Omega)$, with equivalent norms.

To pursue the local minima of L_{PK} , by some direct calculations (more details can be found in Appendix A), we have that the first derivative of L_{PK} on $\theta_j, j = 1, \dots, q$ is

$$(3.9) \quad \frac{\partial}{\partial \theta_j} L_{PK}(\boldsymbol{\theta}) = \frac{\partial \mathbf{b}_\theta^T \mathbf{E}_\theta^{-1} \mathbf{b}_\theta}{\partial \theta_j} + O_p(n^{-\frac{m}{2m+d}}),$$

where \mathbf{E}_θ is defined as (3.5) and $\mathbf{b}_\theta^T = \langle \hat{\zeta}(\cdot) - y^s(\cdot, \boldsymbol{\theta}), \frac{\partial y^s(\cdot, \boldsymbol{\theta})}{\partial \boldsymbol{\theta}} \rangle_{L_2(\Omega)}$. Combing (3.9) with Theorem (3.2), we have the convergence of $\frac{\partial}{\partial \theta_j} L_{PK}(\boldsymbol{\theta})$.

Theorem 3.4. *Under the conditions of Theorem (3.2), if the sample size $n \rightarrow \infty$, we have that*

$$(3.10) \quad \sup_{\boldsymbol{\theta} \in \Theta} \left\| \frac{\partial L_{PK}(\boldsymbol{\theta})}{\partial \theta_j} - \frac{\partial \mathbf{a}_\theta^T \mathbf{E}_\theta^{-1} \mathbf{a}_\theta}{\partial \theta_j} \right\| = 0, j = 1, 2, \dots, q,$$

where $\mathbf{a}_\theta^T = \langle \delta^\theta(\cdot), \frac{\partial y^s(\cdot, \boldsymbol{\theta})}{\partial \boldsymbol{\theta}} \rangle_{L_2(\Omega)}$.

Denote $\boldsymbol{\theta}^s$ as a stationary point of the L_2 loss function, the first derivative of $L_2(\boldsymbol{\theta})$ at $\boldsymbol{\theta}^s$ is zero, that is, $\mathbf{a}_{\boldsymbol{\theta}^s} = \mathbf{0}$. From Theorem 3.4, we can easily have that, $\lim_{n \rightarrow \infty} \frac{\partial L_{PK}(\boldsymbol{\theta})}{\partial \boldsymbol{\theta}} |_{\boldsymbol{\theta}^s} = \mathbf{0}$, i.e. $\boldsymbol{\theta}^s$ is a stationary point of the PK loss function.

To check whether $\boldsymbol{\theta}^s$ is a local maximum or a local minimum of the PPK loss function, the Hessian matrix of $L_{PK}(\boldsymbol{\theta})$ at $\boldsymbol{\theta}^s$, denotes as $\mathbf{H}_{PK}(\boldsymbol{\theta}^s)$, is evaluated from (3.9),

$$(3.11) \quad \mathbf{H}_{PK}(\boldsymbol{\theta}^s) = \frac{\partial \mathbf{b}_{\boldsymbol{\theta}^s}^T \mathbf{E}_{\boldsymbol{\theta}^s}^{-1} \partial \mathbf{b}_{\boldsymbol{\theta}^s}^T}{\partial \boldsymbol{\theta}} + O_p(n^{-\frac{m}{2m+d}}).$$

By the condition A5, $\mathbf{E}_{\boldsymbol{\theta}^s}^{-1}$ is a positive definite matrix, then $\frac{\partial \mathbf{b}_{\boldsymbol{\theta}^s}^T \mathbf{E}_{\boldsymbol{\theta}^s}^{-1} \partial \mathbf{b}_{\boldsymbol{\theta}^s}^T}{\partial \boldsymbol{\theta}} \geq 0$. When the sample size n tends to infinity, we can easily have the following theorem.

Theorem 3.5. *Under the condition of Lemma 3.2, we have that if $\boldsymbol{\theta}^s$ is a local maxima or local minima of the L_2 loss function, then the Hessian matrix of PK loss at $\boldsymbol{\theta}^s$ is positive definite.*

It suggests that the local optimal points of the L_2 loss function are local minima of the PK loss function. Specifically, if $l = 1$, then $\boldsymbol{\theta}_1^s$ is the global minimum of L_{PK} . If $l \geq 2$, then $\boldsymbol{\theta}_1^s, \dots, \boldsymbol{\theta}_l^s$ are local minima of L_{PK} .

3.2. Convergence of the PK loss function. From Theorem 3.2, $\lim_{n \rightarrow \infty} \hat{\delta}_{PK}^{\boldsymbol{\theta}^*}(\cdot) = \zeta(\cdot) - y^s(\cdot, \boldsymbol{\theta}^*) = \delta(\cdot)$. Together with the definition of $L_{PK}(\boldsymbol{\theta})$ and $\|\delta\|_{\mathcal{N}_{K_{\boldsymbol{\theta}^*}}(\Omega)}^2 = O_p(1)$, we have $\lim_{n \rightarrow \infty} L_{PK}(\boldsymbol{\theta}^*) = \sigma^2 + O_p(\lambda) < \infty$. Denote $\lim_{n \rightarrow \infty} L_{PK}(\boldsymbol{\theta}^*) = C < \infty$, the uniform convergence of $\frac{\partial L_{PK}(\boldsymbol{\theta})}{\partial \theta_j}, j = 1, \dots, q$ and the convergence of $L_{PK}(\boldsymbol{\theta}^*)$ guarantee the uniform convergence of $L_{PK}(\boldsymbol{\theta})$, that is

$$(3.12) \quad \sup_{\boldsymbol{\theta} \in \Theta} \|L_{PK}(\boldsymbol{\theta}) - \mathbf{a}_\theta^T \mathbf{E}_\theta^{-1} \mathbf{a}_\theta - C\| = 0, j = 1, 2, \dots, q.$$

Because $\mathcal{P}_{\mathcal{G}_\theta} \delta^\theta = \mathbf{a}_\theta^T \mathbf{E}_\theta^{-1} \frac{\partial y^s(\cdot, \theta)}{\partial \theta^T}$, it follows from basic linear algebra that

$$(3.13) \quad \mathbf{a}_\theta^T \mathbf{E}_\theta^{-1} \mathbf{a}_\theta = \langle \delta^\theta, \mathcal{P}_{\mathcal{G}_\theta} \delta^\theta \rangle_{L_2(\Omega)} = \|\mathcal{P}_{\mathcal{G}_\theta} \delta^\theta\|_{L_2(\Omega)}^2.$$

Combining (3.13) and (3.12), Proposition 3.6 suggests the uniform convergence of $L_{PK}(\boldsymbol{\theta})$.

Theorem 3.6. *Under the condition of Theorem 3.2, if the sample size $n \rightarrow \infty$, we have that*

$$(3.14) \quad \sup_{\boldsymbol{\theta} \in \Theta} \left\| L_{PK}(\boldsymbol{\theta}) - \|\mathcal{P}_{\mathcal{G}_\theta} \delta^\theta\|_{L_2(\Omega)}^2 - C \right\| = 0, j = 1, 2, \dots, q,$$

$\|\mathcal{P}_{\mathcal{G}_\theta} \delta^\theta\|_{L_2(\Omega)}^2 + C$ is named as *projected kernel L_2 loss function (PKL2 loss function)*.

Remark 3.7. Suppose L_2 loss function has l local optima, denoted as $\{\boldsymbol{\theta}_1^s, \dots, \boldsymbol{\theta}_l^s\}$, then Theorem 3.6 suggests that $\lim_{n \rightarrow \infty} L_{PK}(\boldsymbol{\theta}_i^s) = C$ for any $i = 1, \dots, l$.

Theorem 3.5 and Theorem 3.6 shows that when sample size is large, all the local minimum values of PK loss functions tend to be the same one. It indicates that the projected kernel calibration may extremely easily get stuck in local minimum or even local maximum of the L_2 loss function.

3.3. Revisit the Example 2 in [3]. To validate our theoretical assertions, the numerical study in [3] is revisited in this subsection. Example 2 in [3] shows that L_{PK} tends to have more local optimal points than the L_2 loss function. In this example, the smoothness of discrepancy function is infinite, whereas [3] choose a Matérn kernel function (2.1) with $\nu = 1/2$ to estimate the discrepancy function. To avoid the effect of inaccuracy of the correlation function, we make some modification to this example.

Suppose the true process is

$$\zeta(x) = x \cos(3x/2) + x, x \in [0, 5].$$

The computer model is

$$y^s(x, \theta) = \sin(\theta x) + \exp(-2|x|), \theta \in [0, 3].$$

By the definition of θ^* (1.3), we have that $\theta^* = 0.371$. Because the smoothness of $\zeta(\cdot) - y^s(\cdot, \theta)$ depends on the smoothness of $\exp(-2|x|)$, we have that the discrepancy function is in the reproduced kernel Hilbert space generated by the Matérn kernel function $K(d; \frac{1}{2}, \frac{1}{2})$, which is equal to the Sobolev space $H^1(\Omega)$.

Let $\{x_1, x_2, \dots, x_n\}$ be the set of the design points, where $x_i = -5 + \frac{10(i-1)}{n-1}$, $i = 1, 2, \dots, n$ and $n = 100$ is the sample size. Suppose the observation error ϵ_i 's are mutually independent and follow from $N(0, 0.2^2)$. By Theorem 3.2, set the tuning parameter $\lambda = \eta n^{-\frac{2}{3}}$ and η is chosen by K -fold cross validation method [5] with $K = 10$. With the help of *caret* Package [7] in R, we have that $\eta = 0.00138$. To illustrate the performance of the projected kernel calibration more clearly, we scale these two loss function to $[0, 1]$ respectively. The scaled value of loss function L is defined as

$$(3.15) \quad \frac{L(\boldsymbol{\theta}) - \min_{\Theta} L(\boldsymbol{\theta})}{\max_{\Theta} L(\boldsymbol{\theta}) - \min_{\Theta} L(\boldsymbol{\theta})}.$$

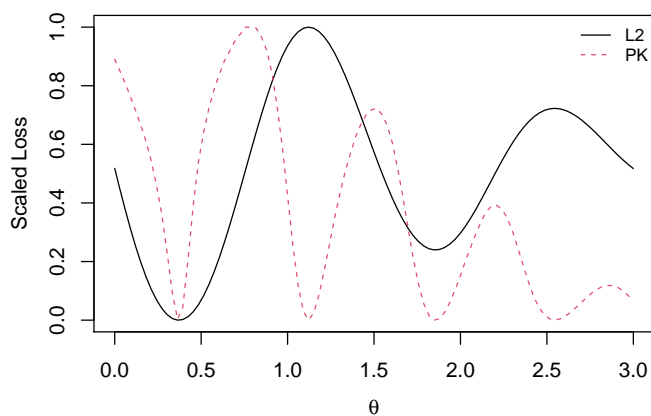


Figure 1. PK loss function (red dashed line) v.s. L_2 loss function (black real line).

Figure 1 shows the comparison between the PK loss function and the L_2 loss function when the sample size $n = 100$. The scaled L_2 loss over $\theta \in [0, 3]$ is shown in the black solid line, which contains a global minimum at 0.371, a local minimum at 1.855, two local maxima at 1.122 and 2.545 respectively. The PK loss function (dashed line) have a global minimum at 0.371, and three local minima at the three local optimal points of the L_2 loss function.

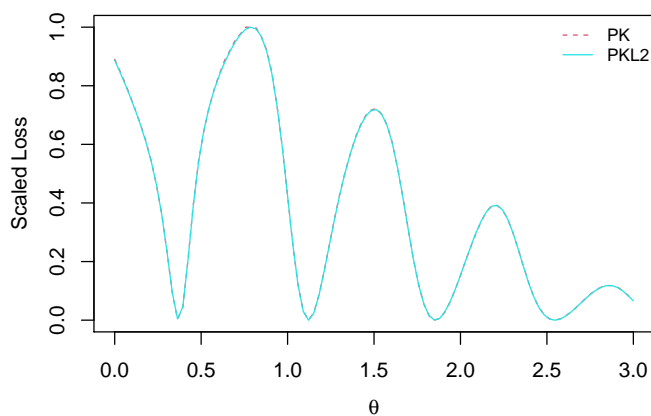


Figure 2. PK loss function (red dashed line) v.s. PKL2 loss function (blue real line).

Figure 2 compares the PK loss function with the PKL2 loss function when the sample size $n = 100$. We can see that the red dashed line is completely coincident with the green real

line. It indicates the PK loss function converges to the PKL2 loss function when the sample size is 100.

4. Penalized projected kernel calibration. The uniform convergence of PK loss function leads to failure of all kinds of global optimization methods. To overcome the problem that the projected kernel calibration faced with, inspired by [3], we scale the L_2 norm of the discrepancy function and introduce a penalized projected kernel calibration method in this section.

4.1. Methodology. Define the penalized projected kernel estimator of $\boldsymbol{\theta}$ as

$$(4.1) \quad \hat{\boldsymbol{\theta}}_{PPK} = \underset{\Theta}{\operatorname{argmin}} \left\{ L_{PK}(\boldsymbol{\theta}) + \eta \|\delta^\theta\|_{L_2(\Omega)}^2 \right\}.$$

Because δ^θ is unknown, a natural choice is replacing δ^θ by its estimator. As Theorem 3.2 provides theoretical guarantee for choosing $\hat{\delta}_{PK}^\theta$ to estimate δ^θ , we propose a two step approach to get $\hat{\boldsymbol{\theta}}_{PPK}$,

- Step 1: For fixed $\boldsymbol{\theta}$, estimate δ^θ by the kernel ridge regression $\hat{\delta}_{PK}^\theta$ (3.1) and λ is chosen by a GCV method;
- Step 2: Plug $\hat{\delta}_{PK}^\theta$ into (4.1), then $\hat{\boldsymbol{\theta}}_{PPK}$ is the minimizer of

$$(4.2) \quad L_{PPK}(\boldsymbol{\theta}) = L_{PK}(\boldsymbol{\theta}) + \eta \|\hat{\delta}_{PK}^\theta\|_{L_2(\Omega)}^2.$$

The loss function (4.2) is named as the *penalized projected kernel loss function* (abbreviated as PPK loss function). By some direct calculations, we have that

$$(4.3) \quad \hat{\boldsymbol{\theta}}_{PPK} = \underset{\Theta}{\operatorname{argmin}} (\mathbf{Y} - \mathbf{Y}_\theta^s)^T \Sigma^{-1} (\mathbf{Y} - \mathbf{Y}_\theta^s),$$

where $\Sigma^{-1} = \left[(\mathbf{K}_\theta + n\lambda \mathbf{I}_n)^{-1} + \gamma (\mathbf{K}_\theta + n\lambda \mathbf{I}_n)^{-1} \|K_\theta(\mathbf{x}, \mathbf{X})\|_{L_2(\Omega)}^2 (\mathbf{K}_\theta + n\lambda \mathbf{I}_n)^{-1} \right]$ and $\gamma = \eta/\lambda$. This expression gives a natural bayesian interpretation of the penalized projected kernel calibration:

$$(4.4) \quad \pi(\boldsymbol{\theta} | \mathbf{Y}, \mathbf{Y}^s) \propto \pi(\boldsymbol{\theta}) \times \exp \left\{ -\frac{1}{2} (\mathbf{Y} - \mathbf{Y}_\theta^s)^T (\mathbf{K}_\theta + n\lambda \mathbf{I}_n)^{-1} (\mathbf{Y} - \mathbf{Y}_\theta^s) \right\},$$

where

$$(4.5) \quad \pi(\boldsymbol{\theta}) \propto \exp \left\{ -\gamma/2 \int_{\Omega} \left(\hat{\delta}_{PK}^\theta(\mathbf{x}) \right)^2 d\mathbf{x} \right\}.$$

We can easily make a comparison between projected kernel calibration and the proposed calibration from their bayesian interpretations (2.7) and (4.4). Based on the definition of $\boldsymbol{\theta}^*$, the estimation of $\boldsymbol{\theta}$ favors to the one where $\|\hat{\delta}_{PK}^\theta\|_{L_2(\Omega)}^2$ is small. The prior distribution $\pi(\boldsymbol{\theta})$ of the proposed method is inversely proportional to $\|\hat{\delta}_{PK}^\theta\|_{L_2(\Omega)}^2$. It is more reasonable than the uninformative prior in (2.7).

4.2. Asymptotic properties. In this section, we investigate the asymptotic properties of the proposed estimator. Firstly, we are concerned with the number of local minima of the PPK loss function. Then, Then, we will show that under certain conditions the proposed estimator of $\boldsymbol{\theta}$ is semi-parametric efficient. Lastly, we focus on the predictive power of the proposed method, in terms of estimating the true process $\zeta(\cdot)$.

Theorem 4.1. *Under the conditions of Theorem 3.2, suppose there exist constants $U \geq L$, such that*

$$U\mathbf{E}_{\theta^s} \geq -\frac{\partial^2 L_2(\boldsymbol{\theta})}{\partial \boldsymbol{\theta} \partial \boldsymbol{\theta}^T} \Big|_{\boldsymbol{\theta}=\boldsymbol{\theta}^s} \geq L\mathbf{E}_{\theta^s}.$$

Suppose $\gamma \in \Gamma_\lambda$, where Γ_λ is presented as

$$(4.6) \quad \Gamma_\lambda = \begin{cases} 0 \leq \gamma < \frac{L}{L+2}/\lambda, & \text{if } L < U \leq -2 \text{ or } L = U < -2, \\ \max(0, \frac{U}{U+2})/\lambda < \gamma < \frac{L}{L+2}/\lambda, & \text{if } L < -2 < U, \\ \gamma > \max(0, \frac{U}{U+2})/\lambda, & \text{if } -2 \leq L < U \text{ or } L = U > -2, \\ \gamma \geq 0, & \text{if } L = U = -2. \end{cases}$$

Then $n \rightarrow \infty$, we have that $\boldsymbol{\theta}^s$ is a local minimum (maximum) of PPK loss function if $\boldsymbol{\theta}^s$ is a local minimum (maximum) of the L_2 loss function.

Theorem 4.2. *Assume that*

B1. $\boldsymbol{\theta}^*$ is the unique solution to (1.3), and is an interior point of Θ .

B2. Assume that

$$V = \int_{\Omega} \frac{\partial^2}{\partial \boldsymbol{\theta}^T \partial \boldsymbol{\theta}} (\zeta(\mathbf{x}) - y^s(\mathbf{x}, \boldsymbol{\theta}^*))^2 d\mathbf{x}$$

is positive definite.

B3. Assume that there exists a neighborhood of $\boldsymbol{\theta}^*$, denoted as Θ' , satisfying

$$\sup_{\boldsymbol{\theta} \in \Theta', j=1,2,\dots,q} \left\{ \left\| \frac{\partial y^s(\cdot, \boldsymbol{\theta})}{\partial \theta_j} \right\|_{\mathcal{N}_{K_\theta}(\Omega)} \right\} < \infty,$$

and

$$\sup_{\boldsymbol{\theta} \in \Theta', 1 \leq i, j \leq q} \left\{ \left\| \frac{\partial^2 y^s(\cdot, \boldsymbol{\theta})}{\partial \theta_i \partial \theta_j} \right\|_{\mathcal{N}_{K_\theta}(\Omega)} \right\} < \infty.$$

Then under the conditions of Theorem 3.2, we have

$$(4.7) \quad \hat{\boldsymbol{\theta}}_{PPK} - \boldsymbol{\theta}^* = -2V^{-1} \left\{ \frac{1}{n} \sum_{i=1}^n e_i \frac{\partial y^s(\mathbf{x}_i, \boldsymbol{\theta}^*)}{\partial \boldsymbol{\theta}} \right\} + o_p(n^{-1/2}).$$

We find that the asymptotic representation of agrees with Theorem 4.3 of [17]. This suggests that the penalized projected kernel calibration also achieves the semi-parametric efficiency.

Theorem 4.3. *Let $\hat{\zeta}_n(\cdot) = \hat{\delta}_{PK}^{\hat{\boldsymbol{\theta}}_{PPK}}(\cdot) + y^s(\cdot, \hat{\boldsymbol{\theta}}_{PPK})$, which is an estimator of $\zeta(\cdot)$. Under the conditions of Theorem 3.2, we have*

$$(4.8) \quad \|\hat{\zeta}_n - \zeta\|_{L_2(\Omega)} = O_p(n^{-\frac{m}{2m+d}}).$$

5. Addressing computational problems. Evaluating $\hat{\theta}_{PPK}$ has two major difficulties in practice. The first problem is the calculations of projected kernels, it is hard to evaluate K_θ from its definition (2.2). The second problem is the choice of γ . We focus on these problems in this section.

5.1. Calculus for projected kernels. A closed form for K_θ is derived in this subsection. Let $\mathbf{g}_\theta^T(\cdot) = \frac{\partial y^s(\cdot, \theta)}{\partial \theta}$ and $\mathbf{h}_\theta(\mathbf{x}) = \langle K(\mathbf{x}, \cdot), \mathbf{g}_\theta(\cdot) \rangle_{L_2(\Omega)}$. By condition A5, \mathbf{E}_θ is positive definite, it follows from basic linear algebra that

$$(5.1) \quad \begin{aligned} \mathcal{P}_{\mathcal{G}_\theta}^{(1)} K(\mathbf{x}_1, \mathbf{x}_2) &= \mathcal{P}_{\mathcal{G}_\theta}^{(2)} K(\mathbf{x}_2, \mathbf{x}_1) = \mathbf{h}_\theta^T(\mathbf{x}_2) \mathbf{E}_\theta^{-1} \mathbf{g}_\theta(\mathbf{x}_1), \\ \mathcal{P}_{\mathcal{G}_\theta}^{(1)} \mathcal{P}_{\mathcal{G}_\theta}^{(2)} K(\mathbf{x}_1, \mathbf{x}_2) &= \mathbf{g}_\theta^T(\mathbf{x}_2) \mathbf{E}_\theta^{-1} \mathbf{H}_\theta \mathbf{E}_\theta^{-1} \mathbf{g}_\theta(\mathbf{x}_1), \end{aligned}$$

where $\mathbf{H}_\theta = \int \int K(\mathbf{t}_1, \mathbf{t}_2) \mathbf{g}_\theta(\mathbf{t}_1) \mathbf{g}_\theta^T(\mathbf{t}_2) d\mathbf{t}_1 d\mathbf{t}_2$. Let $\mathbf{w}_\theta(\mathbf{x}) = \mathbf{H}_\theta \mathbf{E}_\theta^{-1} \mathbf{g}_\theta(\mathbf{x}) - \mathbf{h}_\theta(\mathbf{x})$, then $K_\theta(\mathbf{x}_1, \mathbf{x}_2)$ (2.2) can be represented as

$$(5.2) \quad K(\mathbf{x}_1, \mathbf{x}_2) + \mathbf{w}_\theta(\mathbf{x}_1)^T \mathbf{H}_\theta^{-1} \mathbf{w}_\theta(\mathbf{x}_2) - \mathbf{h}_\theta^T(\mathbf{x}_1) \mathbf{H}_\theta^{-1} \mathbf{h}_\theta(\mathbf{x}_2).$$

Tuo [17] points out that, projected kernel calibration is similar with the bayesian calibration method proposed by [9], which is based on an orthogonal Gaussian process (OGP) modeling technique. The covariance function of an orthogonal Gaussian process which is defined as (5.3) is a projected kernel function.

$$(5.3) \quad K_{or}(\mathbf{x}_1, \mathbf{x}_2) = K(\mathbf{x}_1, \mathbf{x}_2) - \mathbf{h}_\theta^T(\mathbf{x}_1) \mathbf{H}_\theta^{-1} \mathbf{h}_\theta(\mathbf{x}_2).$$

By comparing (5.2) with (5.3), we have that, if and only if $\mathbf{w}_\theta(\mathbf{x}) = \mathbf{0}$, there is $K_\theta = K_{or}$. To address the difficult integrations, we refer to [9] and approximate $\langle f_1, f_2 \rangle_{L_2(\Omega)}$ by

$$(5.4) \quad \frac{1}{N} \sum_{k=1}^N f_1(\xi_k) f_2(\xi_k),$$

where ξ_k 's are independent random samples from the uniform distribution over Ω . By the strong law of large numbers, (5.4) almost surely converges to $\langle f_1, f_2 \rangle_{L_2(\Omega)}$ as $N \rightarrow \infty$. Through this approximation, $\mathbf{h}_\theta(\mathbf{x})$, \mathbf{E}_θ^{-1} and \mathbf{H}_θ can be represented as

$$(5.5) \quad \begin{aligned} \mathbf{h}_\theta(\mathbf{x}) &= \frac{1}{N} \sum_{k=1}^N K(\mathbf{x}, \xi_k) \mathbf{g}_\theta(\xi_k), \\ \mathbf{E}_\theta &= \frac{1}{N} \sum_{k=1}^N \mathbf{g}_\theta(\xi_k) \mathbf{g}_\theta^T(\xi_k), \\ \mathbf{H}_\theta &= \frac{1}{N^2} \sum_{i=1}^N \sum_{j=1}^N K(\xi_i, \xi_j) \mathbf{g}_\theta(\xi_i) \mathbf{g}_\theta^T(\xi_j). \end{aligned}$$

5.2. Choice of γ . Because η is a tuning parameter that effects the number of local optima of $L_{PPK}(\boldsymbol{\theta})$. By increasing η from 0 to ∞ , $L_{PPK}(\boldsymbol{\theta})$ can be gradually tuned from rugged to smooth. In this subsection, a BIC-type criterion is introduced to choose η .

Let $\text{RI}(L)$ be an indicator that measure the ruggedness of a loss function L , such as the number of local optimal points. This indicator satisfies that:

- $\text{RI}(L) \geq 0$, and the equality holds if and only if the loss function L is a nonnegative constant;
- $\text{RI}(cL) = \text{RI}(L)$, where $c > 0$ is a constant;
- $\text{RI}(L + c') = \text{RI}(L)$, where $c' > 0$ is a constant;
- If $\text{RI}(L_1) \leq \text{RI}(L_2)$ then $\text{RI}(L_1) \leq \text{RI}(L_1 + L_2) \leq \text{RI}(L_2)$.

From Theorem 3.5, we have that when the L_2 loss function has more than one local optimal point, $L_{PK}(\boldsymbol{\theta})$ tends to have more local optimal points than $\|\hat{\delta}_{PK}^\theta\|_{L_2(\Omega)}^2$. Therefore, it is easy to be seen that, $\text{RI}(L_{PK}(\boldsymbol{\theta})) \geq \text{RI}(L_{PPK}(\boldsymbol{\theta})) \geq \text{RI}(\|\hat{\delta}_{PK}^\theta\|_{L_2(\Omega)}^2)$ and $\text{RI}(L_{PPK})$ will decrease with the increasing of η . Thus, we use a BIC-type criterion to estimate η

$$(5.6) \quad \eta = \underset{\eta}{\operatorname{argmin}} \log(L_{PK}(\hat{\boldsymbol{\theta}}_{PPK})) + \text{RI}(L_{PPK}) \log(n)/n.$$

In the research on optimization, there are many indicators that can be used to measure the smoothness or ruggedness of the objective function [16]. A natural choice among these indicators is the number of local optima of the objective function. Abbreviating the number of local optima of the loss function L as $NLO(L)$, we have that

$$(5.7) \quad NLO(L) = \#\{\boldsymbol{\theta} : \frac{\partial L(\boldsymbol{\theta})}{\partial \boldsymbol{\theta}^T} = \mathbf{0}\}.$$

In most cases, there is no closed form of $\frac{\partial L(\boldsymbol{\theta})}{\partial \boldsymbol{\theta}^T}$. We use a numerical gradient [15] to approximate the first derivative of L on $\boldsymbol{\theta}$. Newton-Raphson method [13] can be used to evaluate the number of local optima of the loss function L . When the tuning parameter η is chosen by the NLO index, L_{PPK} is named as PPK.NLO loss function.

Note the fact that, when the dimension of $\boldsymbol{\theta}$ is large, it is always hard to count the number of local optimal points for a loss function. An amplitude index, which is an indicator to measure the distribution of local minima of the loss function L , is widely used to assess the ruggedness of a function [16]. This amplitude index is defined as

$$(5.8) \quad \text{Amp}(L) = \frac{\max_{\boldsymbol{\theta}} L(\boldsymbol{\theta}) - \min_{\boldsymbol{\theta}} L(\boldsymbol{\theta})}{\int_{\Theta} L(\boldsymbol{\theta}) - \min_{\boldsymbol{\theta}} L(\boldsymbol{\theta}) d\boldsymbol{\theta}}.$$

The larger $\text{Amp}(L)$ is, the harder is to find the optimal point for the loss function L . The PPK loss function where η is chosen by the Amp index is called PPK.Amp loss function. Denote $\Theta_s = \{\boldsymbol{\theta}_1, \dots, \boldsymbol{\theta}_{N'}\}$ is a discrete set of $\boldsymbol{\theta}$, where $\boldsymbol{\theta}_k, k = 1, \dots, N'$ is randomly sampled from the uniform distribution over Θ . We approximate $\text{Amp}(L)$ by

$$(5.9) \quad \frac{\max_{\Theta_s} L(\boldsymbol{\theta}) - \min_{\Theta_s} L(\boldsymbol{\theta})}{\frac{1}{N'} \sum_{i=1}^{N'} [L(\boldsymbol{\theta}_i) - \min_{\Theta_s} L(\boldsymbol{\theta})]}.$$

6. Numerical studies. In this section, we exam the performance of the penalized projected kernel calibration by using two simulated examples and a real case study. In subsection 6.1, we review example 3.3 and in subsection 6.2, we study a simulated example with two-dimensional calibration parameters. We compare the performance of the penalized projected kernel calibration with some common used calibration methods under different sample sizes. To maintain a fair comparison, the mean function, correlation function, as well as the $\{\xi_j\}$'s in the integration are all set to be the same.

6.1. Review of example 3.3. To exam the performance of the proposed method, we compare the PPK loss function with the L_2 loss function and the PK loss function both when the sample sizes are $n = \{6, 15, 100\}$. The physical design and kernel function are set to be the same as example 3.3. The tuning parameter η in the PPK loss function is chosen by the BIC-type criterion (5.6). We use two indexes $NLO(L)$ and $Amp(L)$ to measure the ruggedness of the loss function.

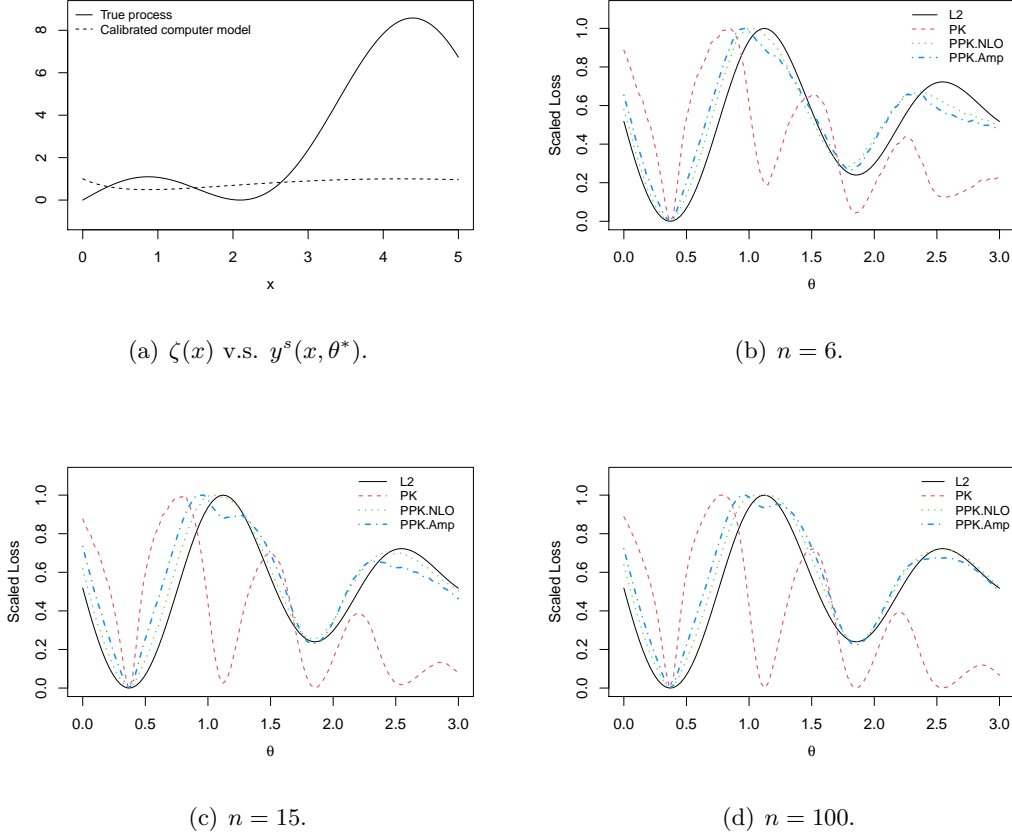


Figure 3. (a) the true process $\zeta(x)$ (black real line) v.s. the calibrated computer model $y^s(x, \theta^*)$ (black dashed line); (b)-(d) L_2 loss function (black real line) v.s. PK loss function (red dashed line) v.s. PPK. NLO loss function (green dotted line) v.s. PPK. Amp loss function (blue dot-dash line).

From Figure 3-(a) we can see that, even though θ^* is the global minima of the $\|\zeta - y^s(\cdot, \theta)\|_{L_2(\Omega)}^2$, the discrepancy between the true process and the calibrated computer model is still large. Figure 3-(b-d) show the comparison of the the L_2 loss function, the PK loss function and the PPK loss function when the sample sizes are 6, 15 and 100. PPK.NLO loss function is the PPK loss function that the NLO index is used to measure the ruggedness of a loss function L , whereas PPK.Amp loss function is the PPK loss function that the Amp index is used. Because the dimension of calibration parameter is one, with the help the package *rootSolve* [13] in R, we can obtain the number of local optimal of the loss function and the estimation of η_{NLO} . Let $\Theta_s = \{\theta_1, \dots, \theta_{N'}\}$ where $\theta_i = \frac{3i}{N'}$ and $N' = 100$. By approximating $Amp(L)$ by (5.9), we have the choice of η_{Amp} . Table 2 shows the choice of η_{NLO} and η_{Amp} with different sample sizes.

Table 2
Choice of η

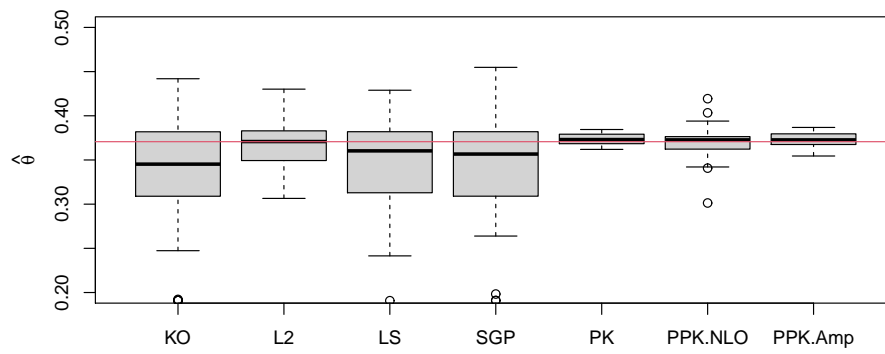
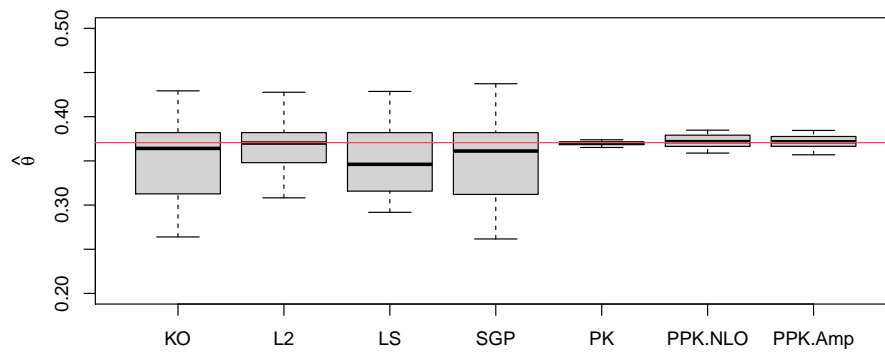
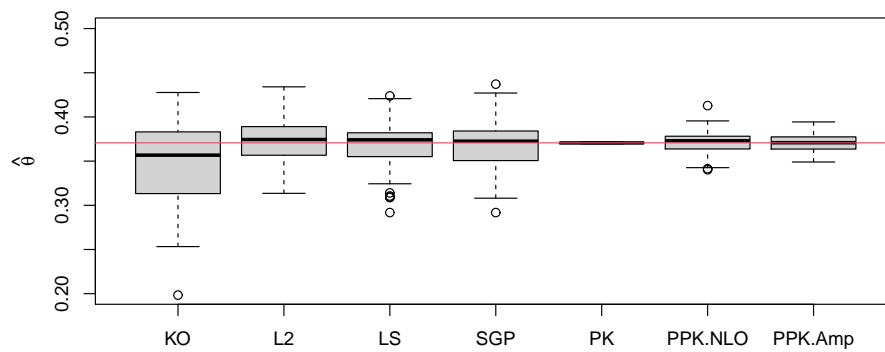
Sample size	η_{NLO}	η_{Amp}
$n = 6$	0.153	0.0503
$n = 15$	0.705	0.236
$n = 100$	13.632	6.477

Figure 3 indicates that when the sample size is larger than 6, the PPK loss function suffers from the multi-optima problem. Figure 3-(b) shows that when the sample size is 6, one may distinguish between the global minimum and the local minimum near 1.855 by an effective optimization algorithm. However, 3-(c-d) show that when the sample size is larger than 15, it becomes extremely hard to find the global minimum by any optimization algorithm. It can be seen from the PPK loss function that the proposed method can solve this problem that PK calibration faced with. The number of local optimal points of the PPK.NLO loss functions are 4, and values of the local minima are different. Although the PPK.Amp loss functions have more than 4 local optimal points, the global minimizer can be evaluated effectively by some optimization method, like the quasi-Newton optimization methods with multiple initial points .

Because $NLO(L)$ counts number of local optimal points of L , the BIC-type criterion favors to η that decrease the number of local optimal points of the PPK loss function. This leads to the fact that η_{NLO} is larger than η_{Amp} as shown in Table 2 and PPK.NLO loss functions have less local optimal points than PPK.Amp loss functions as shown in Figure 3. Moreover, η_{NLO} and η_{Amp} are increasing when the sample size becomes large. The reason is that it becomes much harder to pick out the global minimum of the PK loss function with the increasing of n .

To compare the performance of the PPK calibration with the KO's calibration (KO), the L_2 calibration (L_2), the least square calibration (LS), the scaled Gaussian process model calibration (SGP) and the projected kernel calibration (PK), we repeat the process of calibration 100 times for each method, and show the box-plots of $\hat{\theta}$ in Figure 4. Because the PK calibration will be easily trapped in a local optimal solution of the PPK loss function, we narrow the search space of the PK calibration to $[0, 0.5]$.

From Figure 4, we can see that, firstly the variance of $\hat{\theta}_{PK}$ is the smallest. In fact, as

(a) $n = 6$.(b) $n = 15$.(c) $n = 100$.**Figure 4.** Estimations of the calibration parameter by different methods.

the PK loss function tends to have more local optima, the PK loss function near its global minimum point is “sharp” (the derivatives near the global minimum point is large). Secondly, the bias of $\hat{\theta}_{PK}$ is near zero. These results indicate that if the search region is narrowed, the PK calibration is obviously superior to other methods. However, when there are many local optimal in the search region, the PK calibration will lose this advantage.

When the sample size is 6 and 15, the the slower convergence speed leads to the poor performance of the $\hat{\theta}_{SGP}$. When the sample size is 100, there is still substantial estimation error in $\hat{\theta}_{KO}$, the reason is that the discrepancy δ is large (see Figure 3-(a)) and $\hat{\theta}_{KO}$ is inconsistent. Denote the estimations given by the PPK.NLO loss function (PPK.Amp loss function) as $\hat{\theta}_{PPK.NLO}$ ($\hat{\theta}_{PPK.Amp}$). We have that the bias of $\hat{\theta}_{PPK}$ is near zero. The variance of $\hat{\theta}_{PPK}$ is smaller than the variance of $\hat{\theta}$ given by other methods except by the PK calibration method. In addition, because the tuning parameter $\eta_{Amp} < \eta_{NLO}$, $\hat{\theta}_{PPK.Amp}$'s are more close to $\hat{\theta}_{PK}$ and the variance of $\hat{\theta}_{PPK.Amp}$ is smaller than the variance of $\hat{\theta}_{PPK.NLO}$. It imply that, the proposed method outperforms other calibration methods.

6.2. Low-accuracy version of the PARK function [27]. Suppose $\zeta(\cdot)$ is the PARK function [8],

$$\zeta(\mathbf{x}) = \frac{x_1}{2} \left[\sqrt{1 + (x_2 + x_3^2) \frac{x_4}{x_1^2}} - 1 \right] + (x_1 + 3x_4) \exp[1 + \sin(x_3)], \mathbf{x} \in [0, 1]^4.$$

For the purpose of multi-fidelity simulation, [27] gives a lower accuracy version of the PARK function. Suppose some constants of this lower fidelity model are needed to be determined, we use following computer model to exam the performance of the proposed method:

$$y^s(\mathbf{x}, \boldsymbol{\theta}) = (\theta_1 + \frac{\sin(x_1)}{10})\zeta(\mathbf{x}) + \theta_2(-2x_1 + x_2^2 + x_3^2) + 0.5,$$

where θ_1 and θ_2 are two calibration parameters, with $\boldsymbol{\theta} \in [-5, 5]^2$.

Let $\mathbf{X} = (\mathbf{x}_1, \dots, \mathbf{x}_n)^T$ be the physical design, which is randomly generated by maximin Latin hypercube design method [11]. Suppose the observation error ϵ_i 's are mutually independent and follow from $N(0, 0.1^2)$. We use a Matérn kernel function (2.1) with $\nu = 7/2$ as the kernel function K . To determine the hyper-parameter ρ in (2.1), for fixed $\boldsymbol{\theta}_0$, we build a Gaussian-process model to approximate $y(\mathbf{x}_i) - y^s(\mathbf{x}_i, \boldsymbol{\theta}_0)$ and estimate ρ by using the maximum likelihood method. Because the least square estimator $\hat{\boldsymbol{\theta}}_{LS}$ which is proposed by [25] is consistent, we denote $\boldsymbol{\theta}_0 = \hat{\boldsymbol{\theta}}_{LS}$.

Contour maps of the L_2 loss function and the PK loss function with $n = \{10, 20, 100\}$ are shown in Figure 5. From the top left subfigure, we can see that, $\boldsymbol{\theta}^*$ is the only one local optimal point of the L_2 loss function. The top right subfigure and the two bottom subfigures imply that the PK loss function has only one local minimum, regardless of whether the sample size is sufficiently large ($n = 100$) or rather small ($n = 10$). It indicates that when the L_2 loss function has only one local optimal point, the PK loss function will not suffer from a multiple local minima problem. Because the L_2 loss function and the PPK loss function are convex, we apply the NEWUOA algorithm [10] to find $\boldsymbol{\theta}^*$ and $\hat{\boldsymbol{\theta}}_{PK}$. In Figure 5, the location of $\boldsymbol{\theta}^* = (0.546, 0.0926)$ is shown by the blue cross and the location of $\hat{\boldsymbol{\theta}}_{PK}$ is shown by the

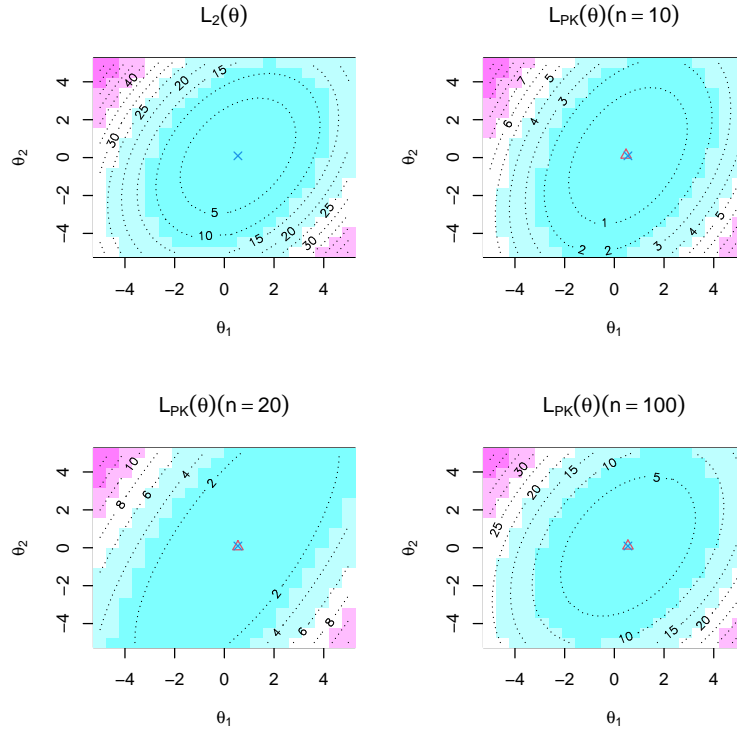


Figure 5. L_2 loss function v.s. PK loss function with $n = \{10, 20, 100\}$ in Example 6.2. The cross in each subfigure is the location of θ^* , and triangle is the location of θ_{PK} .

red triangle. By comparing the locations of three red triangles with location of the blue cross (location of θ^*), we have that, $\hat{\theta}_{PK}$ is almost equal to θ^* especially then n is large.

To compare the performance of the proposed method with some existing calibration methods, we repeat the simulation procedure 100 times to assess the average performance of different methods.

Figure 6 compares the estimation of the calibration parameters by different calibration methods. Because there is only one local optimal point in the PK loss function, the choice of η is zero, therefore $\hat{\theta}_{PPK} = \hat{\theta}_{PK}$. We can see that when the sample size is 10 and 20, the bias of $\hat{\theta}_{PK}$ is smallest, whereas the variance of $\hat{\theta}_{PK}$ is a little larger than $\hat{\theta}_{LS}$. When the sample size is 100, all the methods perform good except the KO's calibration.

6.3. Spot welding example. Now we consider the spot welding example studied in [1] and [26]. Same as [26], we consider two control variables in this example: the load and the current. Besides the control variables in the physical experiment, the computer model (a Finite Element model) also involves a calibration parameter (denoted as u in [1]). Details of the inputs and outputs of the computer experiments are listed in Table 3. The physical data are provided in Table 4 of [1]. There are 21 available runs for the computer code, as presented in Table 3 of [1]. With the help of RobustGaSP package [2] in R, a gaussian process model is built to approximate the computer outputs. In the process of calibration, the Finite Element

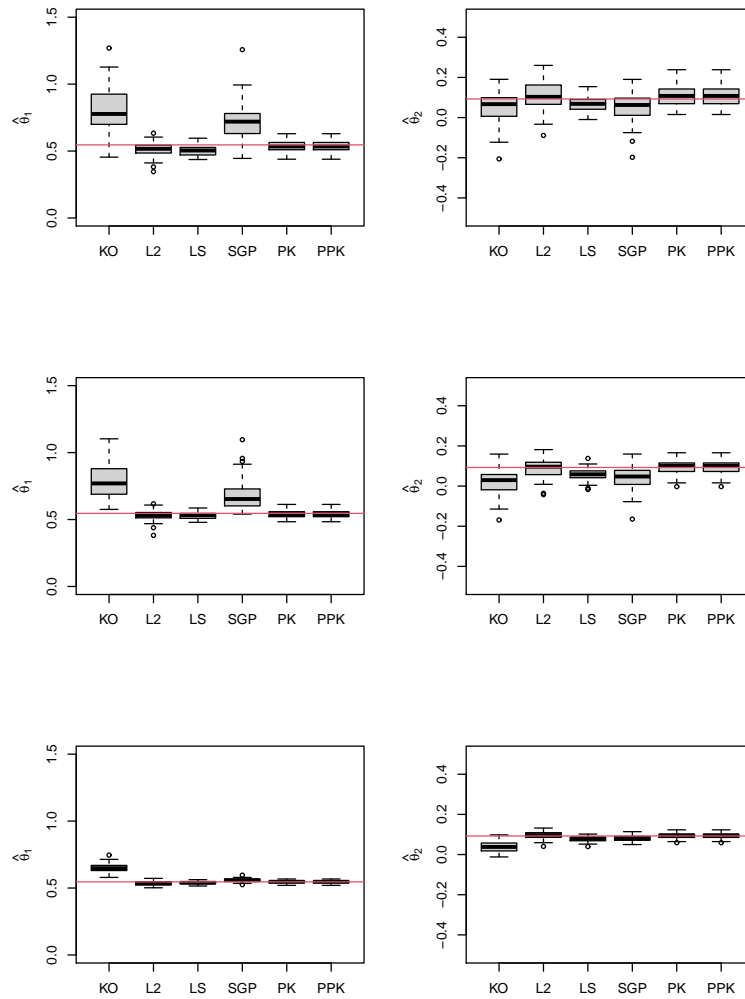


Figure 6. Comparisons of different calibration methods with the sample size $n = 10$ (the first row), $n = 20$ (the second row) and $n = 100$ (the third row).

Table 3
Inputs and output of the computer experiments

Inputs		
C (current)	[23, 30]	control variable
L (load)	[3.8, 5.5]	control variable
θ (contact resistance)	[0.8, 8]	calibration parameter
Output	Size of the nugget after 8-cycles	

model is replaced by the predictive mean of the RobustGaSP emulator. Because there is only one local optimal point in the PK loss function, similar with Subsection 6.2, we have that the tuning parameter is $\eta = 0$.

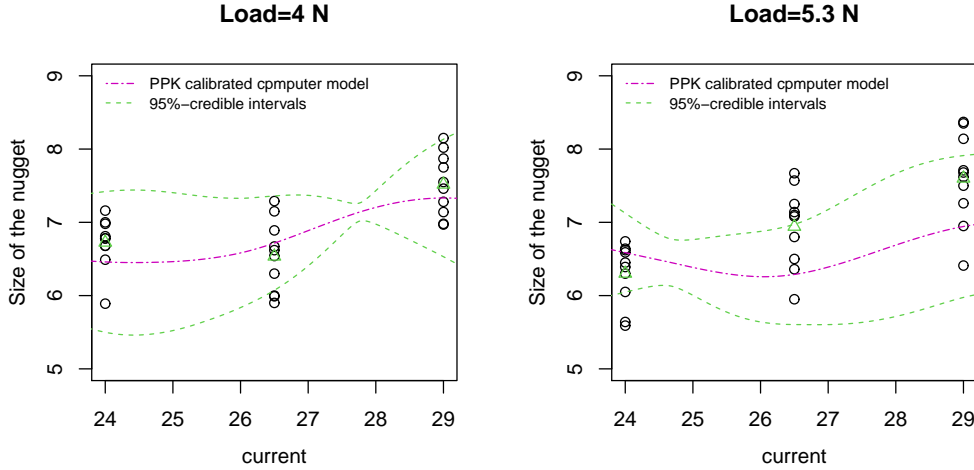


Figure 7. Physical observations (black circles); mean of physical observations for a fixed current (green triangles); mean of the calibrated computer model by the proposed method (red real line) and the 95% interval of the calibrated computer model (green dashed line).

The computer models calibrated by the proposed method, together with their corresponding point-wise 95%-credible intervals, are depicted in Figure 7. We can see that the proposed method can give a good calibrated computer model.

7. Discussion. In this work, we prove that the projected kernel calibration is extremely easy to be trapped in a local minimum even a local maximum of the L_2 loss between the true process and the computer model. A frequentist calibration method is proposed to overcome this problem. Estimator of the calibration parameter given by the proposed method is proven to be consistent and semi-parametric efficient. Numerical examples are studied to compare the proposed methods with some existing calibration methods. The results show that the proposed method outperform other methods.

Appendix A. Technical proofs in Section 2 .

proof of Theorem 3.1 . Following from the representer's Theorem, we find that $\hat{\delta}^\theta$ can be expressed by

$$\hat{\delta}^\theta = \sum_{i=1}^n c_i^\theta K_\theta(x - x_i),$$

with $c^\theta = (c_1^\theta, \dots, c_n^\theta)^T$ defined as

$$c = (\mathbf{K}_\theta + n\lambda\mathbf{I}_n)^{-1}\Delta^\theta,$$

where $\Delta^\theta = (\delta_1^\theta, \dots, \delta_n^\theta)^T$. The norm of $\hat{\delta}^\theta$ in $\mathcal{N}_{K_\theta}(\Omega)$ is given by

$$(A.1) \quad \|\hat{\delta}^\theta\|_{\mathcal{N}_{K_\theta}(\Omega)}^2 = \Delta_\theta^T (\mathbf{K}_\theta + n\lambda \mathbf{I}_n)^{-1} \mathbf{K}_\theta (\mathbf{K}_\theta + n\lambda \mathbf{I}_n)^{-1} \Delta_\theta.$$

Also, $\hat{\Delta}^\theta := (\hat{\delta}^\theta(x_1), \dots, \hat{\delta}^\theta(x_n))^T$ can be expressed by

$$\hat{\Delta}^\theta = \mathbf{K}_\theta (\mathbf{K}_\theta + n\lambda \mathbf{I}_n)^{-1} \Delta_\theta,$$

which yields

$$\begin{aligned} \Delta_\theta - \hat{\Delta}^\theta &= (I - \mathbf{K}_\theta (\mathbf{K}_\theta + n\lambda \mathbf{I}_n)^{-1}) \Delta_\theta \\ &= n\lambda (\mathbf{K}_\theta + n\lambda \mathbf{I}_n)^{-1} \Delta_\theta. \end{aligned}$$

Thus

$$(A.2) \quad \frac{1}{n} \sum_{i=1}^n (\delta_i^\theta - \hat{\delta}^\theta(x_i))^2 = n\lambda^2 \Delta_\theta^T (\mathbf{K}_\theta + n\lambda \mathbf{I}_n)^{-2} \Delta_\theta.$$

From (A.1) and (A.2) we obtain

$$\frac{1}{n} \sum_{i=1}^n (\delta_i^\theta - \hat{\delta}^\theta(x_i))^2 + \lambda \|\hat{\delta}^\theta\|_{\mathcal{N}_{K_\theta}(\Omega)}^2 = \lambda \Delta_\theta^T (\mathbf{K}_\theta + n\lambda \mathbf{I}_n)^{-1} \Delta_\theta,$$

which implies the desired results. ■

proof of Theorem 3.2. Based on the definition of kernel ridge regression, $\hat{\delta}_{PK}^\theta$ is a minimizer of

$$(A.3) \quad \operatorname{argmin}_{f \in \mathcal{N}_{K_\theta}(\Omega)} \frac{1}{n} \sum_{i=1}^n (y_i - y^s(\mathbf{x}_i, \theta) - f)^2 + \lambda \|f\|_{\mathcal{N}_{K_\theta}(\Omega)}^2,$$

We have the basic inequality

$$(A.4) \quad \begin{aligned} &\frac{1}{n} \sum_{i=1}^n \left(\delta^\theta(\mathbf{x}_i) - \hat{\delta}_{PK}^\theta(\mathbf{x}_i) \right)^2 + \lambda \|\hat{\delta}_{PK}^\theta\|_{\mathcal{N}_{K_\theta}(\Omega)}^2 \\ &\leq \lambda \|\delta^\theta\|_{\mathcal{N}_{K_\theta}(\Omega)}^2 + \frac{2}{n} \sum_{i=1}^n e_i \left(\hat{\delta}_{PK}^\theta(\mathbf{x}_i) - \delta^\theta(\mathbf{x}_i) \right) \end{aligned}$$

Following from the Theorem 5.11 in [21], we obtain the modulus of continuity of the empirical process $v(g') = \langle e, g' - g \rangle_n$ as

$$(A.5) \quad \sup_{g \in \mathcal{N}_K(\Omega)} \frac{\langle e, g' - g \rangle_n}{\|g - g'\|_n^{1-\frac{d}{2m}} \|g'\|_{\mathcal{N}_K(\Omega)}^{d/2m}} = O_p(n^{-1/2}).$$

That is

$$(A.6) \quad \begin{aligned} &|\langle e, \hat{\delta}_{PK}^\theta(\mathbf{x}_i) - \delta^\theta(\mathbf{x}_i) \rangle_n| \\ &\leq O_p(n^{-1/2}) \left\| \hat{\delta}_{PK}^\theta(\mathbf{x}_i) - \delta^\theta(\mathbf{x}_i) \right\|_n^{1-\frac{d}{2m}} \left\| \hat{\delta}_{PK}^\theta(\mathbf{x}_i) \right\|_{\mathcal{N}_K(\Omega)}^{d/2m}. \end{aligned} \quad \blacksquare$$

By combining (A.4), (A.6) with the Theorem 3.3 of [17], and by using the arguments similar to the proof of Theorem 10.2 of [21], we can obtain the desired results.

Proof of Theorem 3.4. From (3.2), the stationary points of PK loss function satisfy that

$$\begin{aligned}
0 &= \frac{\partial}{\partial \theta_j} \left\{ \frac{1}{n} \sum_{i=1}^n \left(\delta_i^\theta - \hat{\delta}_{PK}^\theta(\mathbf{x}_i) \right)^2 + \lambda \|\hat{\delta}_{PK}^\theta\|_{\mathcal{N}_{K_\theta}(\Omega)}^2 \right\} \\
&= \frac{2}{n} \sum_{i=1}^n \left(\delta_i^\theta - \hat{\delta}_{PK}^\theta(\mathbf{x}_i) \right) \frac{\partial \left(\delta_i^\theta - \hat{\delta}_{PK}^\theta(\mathbf{x}_i) \right)}{\partial \theta_j} + \lambda \frac{\partial \|\hat{\delta}_{PK}^\theta\|_{\mathcal{N}_{K_\theta}(\Omega)}^2}{\partial \theta_j}
\end{aligned}
\tag{A.7}$$

It is easily seen that

$$\frac{\partial \delta_i^\theta}{\partial \theta_j} = - \frac{\partial y^s(\mathbf{x}_i, \boldsymbol{\theta})}{\partial \theta_j}.
\tag{A.8}$$

Next, we need to compute the partial derivative of $\hat{\delta}_{PK}^\theta$ and $\|\hat{\delta}_{PK}^\theta\|_{\mathcal{N}_{K_\theta}(\Omega)}^2$ of $\theta_j, j \in \{1, 2, \dots, q\}$. Because $\mathcal{P}_{G_\theta} \hat{\delta}^\theta = \mathbf{b}_\theta^T \mathbf{E}_\theta^{-1} \mathbf{g}_\theta$, where $\mathbf{b}_\theta^T = \left(\int_\Omega (\hat{\zeta} - y^s(\mathbf{x}, \boldsymbol{\theta})) \frac{\partial y^s(\mathbf{x}, \boldsymbol{\theta})}{\partial \theta_1} d\mathbf{x}, \int_\Omega (\hat{\zeta} - y^s(\mathbf{x}, \boldsymbol{\theta})) \frac{\partial y^s(\mathbf{x}, \boldsymbol{\theta})}{\partial \theta_2} d\mathbf{x}, \dots, \int_\Omega (\hat{\zeta} - y^s(\mathbf{x}, \boldsymbol{\theta})) \frac{\partial y^s(\mathbf{x}, \boldsymbol{\theta})}{\partial \theta_q} d\mathbf{x} \right)$, we have

$$\begin{aligned}
\frac{\partial \hat{\delta}_{PK}^\theta}{\partial \theta_j} &= \frac{\partial (\hat{\delta}^\theta - \mathcal{P}_{G_\theta} \hat{\delta}^\theta)}{\partial \theta_j}, \\
&= - \frac{\partial y^s(\mathbf{x}_i, \boldsymbol{\theta})}{\partial \theta_j} - \frac{\partial \mathbf{b}_\theta^T \mathbf{E}_\theta^{-1} \mathbf{g}_\theta}{\partial \theta_j}, \\
&= - \frac{\partial y^s(\mathbf{x}_i, \boldsymbol{\theta})}{\partial \theta_j} - \frac{\partial \mathbf{b}_\theta^T}{\partial \theta_j} \mathbf{E}_\theta^{-1} \mathbf{g}_\theta - \mathbf{b}_\theta^T \frac{\partial \mathbf{E}_\theta^{-1}}{\partial \theta_j} \mathbf{g}_\theta - \mathbf{b}_\theta^T \mathbf{E}_\theta^{-1} \frac{\partial \mathbf{g}_\theta}{\partial \theta_j}.
\end{aligned}
\tag{A.9}$$

From Lemma 6.6 of [17], we have that

$$\frac{\partial \|\hat{\delta}_{PK}^\theta\|_{\mathcal{N}_{K_\theta}(\Omega)}^2}{\partial \theta_j} = O_p(1).
\tag{A.10}$$

Because $\int \hat{\delta}_{PK}^\theta \mathbf{g}_\theta d\mathbf{x} = 0$, by using (3.7), we have $\frac{1}{n} \sum_{i=1}^n \hat{\delta}_{PK}^\theta(\mathbf{x}_i) \mathbf{g}_\theta(\mathbf{x}_i) = o_p(n^{-1/2})$. Invoking the condition that $\lambda \sim n^{-\frac{2m}{2m+d}}$ and combining (A.7) -(A.10), we have that the partial derivative of the PK loss function is

$$\begin{aligned}
&\frac{2}{n} \sum_{i=1}^n \left(\delta_i^\theta - \hat{\delta}_{PK}^\theta(\mathbf{x}_i) \right) \frac{\partial \left(\delta_i^\theta - \hat{\delta}_{PK}^\theta(\mathbf{x}_i) \right)}{\partial \theta_j} + o_p(n^{-1/2}) \\
&= \frac{\partial \mathbf{b}_\theta^T}{\partial \theta_j} \mathbf{E}_\theta^{-1} \frac{2}{n} \sum_{i=1}^n \delta_i^\theta \mathbf{g}_\theta(\mathbf{x}_i) + \mathbf{b}_\theta^T \frac{\partial \mathbf{E}_\theta^{-1}}{\partial \theta_j} \frac{2}{n} \sum_{i=1}^n \delta_i^\theta \mathbf{g}_\theta(\mathbf{x}_i) + \mathbf{b}_\theta^T \mathbf{E}_\theta^{-1} \frac{2}{n} \sum_{i=1}^n \delta_i^\theta \frac{\partial \mathbf{g}_\theta(\mathbf{x}_i)}{\partial \theta_j} \\
&\quad - \mathbf{b}_\theta^T \mathbf{E}_\theta^{-1} \frac{2}{n} \sum_{i=1}^n \hat{\delta}_{PK}^\theta(\mathbf{x}_i) \frac{\partial \mathbf{g}_\theta(\mathbf{x}_i)}{\partial \theta_j} + o_p(n^{-1/2}).
\end{aligned}
\tag{A.11}$$

By the definition of δ_i^θ , it is easily obtained that

$$\begin{aligned}
\frac{1}{n} \sum_{i=1}^n \delta_i^\theta \mathbf{g}_\theta(\mathbf{x}_i) &= \frac{1}{n} \sum_{i=1}^n (\zeta_i - y^s(\mathbf{x}_i, \boldsymbol{\theta}) + e_i) \mathbf{g}_\theta(\mathbf{x}_i) \\
\text{(A.12)} \quad &= \frac{1}{n} \sum_{i=1}^n (\hat{\zeta}_i - y^s(\mathbf{x}_i, \boldsymbol{\theta}) + \zeta_i - \hat{\zeta}_i + e_i) \mathbf{g}_\theta(\mathbf{x}_i) \\
&= \frac{1}{n} \sum_{i=1}^n (\hat{\zeta}_i - y^s(\mathbf{x}_i, \boldsymbol{\theta})) \mathbf{g}_\theta(\mathbf{x}_i) + \frac{1}{n} \sum_{i=1}^n (\zeta_i - \hat{\zeta}_i) \mathbf{g}_\theta(\mathbf{x}_i) + \frac{1}{n} \sum_{i=1}^n e_i \mathbf{g}_\theta(\mathbf{x}_i)
\end{aligned}$$

Because $\mathcal{N}_{K_\theta}(\Omega)$ can be continuously embedded into the Sobolev space $H^m(\Omega)$, we use Theorem 5.11 of [21] to obtain that $\frac{1}{\sqrt{n}} \sum_{i=1}^n e_i \mathbf{g}_\theta(\mathbf{x}_i) = O_p(1)$. Moreover, by Cauchy-schwarz inequality, we have $\frac{1}{n} \sum_{i=1}^n (\zeta_i - \hat{\zeta}_i) \mathbf{g}_\theta(\mathbf{x}_i) = \langle \zeta - \hat{\zeta}, \mathbf{g}_\theta \rangle_n \leq \|\zeta - \hat{\zeta}\|_n \|\mathbf{g}_\theta\|_n$. From the Theorem 4.1 of [17], $\|\zeta - \hat{\zeta}\|_n = O_p(n^{-\frac{m}{2m+d}})$. By combining with (3.7), we obtained that

$$\text{(A.13)} \quad \frac{1}{n} \sum_{i=1}^n \delta_i^\theta \mathbf{g}_\theta(\mathbf{x}_i) = \mathbf{b}_\theta + O_p(n^{-\frac{m}{2m+d}}).$$

Similarly,

$$\begin{aligned}
\frac{1}{n} \sum_{i=1}^n \delta_i^\theta \frac{\partial \mathbf{g}_\theta(\mathbf{x}_i)}{\partial \theta_j} &= \frac{1}{n} \sum_{i=1}^n (\zeta_i - y^s(\mathbf{x}_i, \boldsymbol{\theta}) + e_i) \frac{\partial \mathbf{g}_\theta(\mathbf{x}_i)}{\partial \theta_j}, \\
\text{(A.14)} \quad &= \int (\hat{\zeta} - y^s(\mathbf{x}, \boldsymbol{\theta})) \frac{\partial \mathbf{g}_\theta(\mathbf{x})}{\partial \theta_j} d\mathbf{x} + O_p(n^{-\frac{m}{2m+d}}), \\
&= \frac{\partial \mathbf{b}_\theta}{\partial \theta_j} + \int \frac{\partial y^s(\mathbf{x}, \boldsymbol{\theta})}{\partial \theta_j} \mathbf{g}_\theta d\mathbf{x} + O_p(n^{-\frac{m}{2m+d}}).
\end{aligned}$$

Because $\int \hat{\delta}_{PK}^\theta \mathbf{g}_\theta d\mathbf{x} = 0$, taking the partial derivative of $\int \hat{\delta}_{PK}^\theta \mathbf{g}_\theta d\mathbf{x}$ of θ_j , we have

$$\text{(A.15)} \quad \int \frac{\partial \hat{\delta}_{PK}^\theta}{\partial \theta_j} \mathbf{g}_\theta d\mathbf{x} + \int \hat{\delta}_{PK}^\theta \frac{\partial \mathbf{g}_\theta}{\partial \theta_j} d\mathbf{x} = 0.$$

Moverover, because $\int \mathbf{g}_\theta \mathbf{g}_\theta^T d\mathbf{x} = \mathbf{E}_\theta$, and $\frac{\partial \mathbf{E}_\theta^{-1}}{\partial \theta_j} = -\mathbf{E}_\theta^{-1} \frac{\partial \mathbf{E}_\theta}{\partial \theta_j} \mathbf{E}_\theta^{-1}$, we have

$$\begin{aligned}
\int \hat{\delta}_{PK}^\theta \frac{\partial \mathbf{g}_\theta}{\partial \theta_j} d\mathbf{x} &= - \int \mathbf{g}_\theta \frac{\partial \hat{\delta}_{PK}^\theta}{\partial \theta_j} d\mathbf{x}, \\
&= \int \mathbf{g}_\theta \left\{ \frac{\partial y^s(\mathbf{x}_i, \boldsymbol{\theta})}{\partial \theta_j} + \frac{\partial \mathbf{b}_\theta^T}{\partial \theta_j} \mathbf{E}_\theta^{-1} \mathbf{g}_\theta + \mathbf{b}_\theta^T \frac{\partial \mathbf{E}_\theta^{-1}}{\partial \theta_j} \mathbf{g}_\theta + \mathbf{b}_\theta^T \mathbf{E}_\theta^{-1} \frac{\partial \mathbf{g}_\theta}{\partial \theta_j} \right\}^T d\mathbf{x}, \\
\text{(A.16)} \quad &= \int \mathbf{g}_\theta \frac{\partial y^s(\mathbf{x}_i, \boldsymbol{\theta})}{\partial \theta_j} d\mathbf{x} + \frac{\partial \mathbf{b}_\theta}{\partial \theta_j} + \mathbf{E}_\theta \frac{\partial \mathbf{E}_\theta^{-1}}{\partial \theta_j} \mathbf{b}_\theta + \int \mathbf{g}_\theta (\frac{\partial \mathbf{g}_\theta}{\partial \theta_j})^T d\mathbf{x} \mathbf{E}_\theta^{-1} \mathbf{b}_\theta, \\
&= \int \mathbf{g}_\theta \frac{\partial y^s(\mathbf{x}_i, \boldsymbol{\theta})}{\partial \theta_j} d\mathbf{x} + \frac{\partial \mathbf{b}_\theta}{\partial \theta_j} + \mathbf{E}_\theta \frac{\partial \mathbf{E}_\theta^{-1}}{\partial \theta_j} \mathbf{b}_\theta + \frac{1}{2} \frac{\partial \mathbf{E}_\theta}{\partial \theta_j} \mathbf{E}_\theta^{-1} \mathbf{b}_\theta, \\
&= \int \mathbf{g}_\theta \frac{\partial y^s(\mathbf{x}_i, \boldsymbol{\theta})}{\partial \theta_j} d\mathbf{x} + \frac{\partial \mathbf{b}_\theta}{\partial \theta_j} + \frac{1}{2} \mathbf{E}_\theta \frac{\partial \mathbf{E}_\theta^{-1}}{\partial \theta_j} \mathbf{b}_\theta.
\end{aligned}$$

Combining (A.13), (A.14) and (A.16), we have that (A.11) can be represented as

$$\begin{aligned}
& 2\frac{\partial \mathbf{b}_\theta^T}{\partial \theta_j} \mathbf{E}_\theta^{-1} \mathbf{b}_\theta + 2\mathbf{b}_\theta^T \frac{\partial \mathbf{E}_\theta^{-1}}{\partial \theta_j} \mathbf{b}_\theta + 2\mathbf{b}_\theta^T \mathbf{E}_\theta^{-1} \left(\frac{\partial \mathbf{b}_\theta}{\partial \theta_j} + \int \frac{\partial y^s(\mathbf{x}, \boldsymbol{\theta})}{\partial \theta_j} \mathbf{g}_\theta d\mathbf{x} \right) \\
\text{(A.17)} \quad & - 2\mathbf{b}_\theta^T \mathbf{E}_\theta^{-1} \left(\int \mathbf{g}_\theta \frac{\partial y^s(\mathbf{x}, \boldsymbol{\theta})}{\partial \theta_j} d\mathbf{x} + \frac{\partial \mathbf{b}_\theta}{\partial \theta_j} + \frac{1}{2} \mathbf{E}_\theta \frac{\partial \mathbf{E}_\theta^{-1}}{\partial \theta_j} \mathbf{b}_\theta \right) + O_p(n^{-\frac{m}{2m+d}}) \\
& = 2\frac{\partial \mathbf{b}_\theta^T}{\partial \theta_j} \mathbf{E}_\theta^{-1} \mathbf{b}_\theta + \mathbf{b}_\theta^T \frac{\partial \mathbf{E}_\theta^{-1}}{\partial \theta_j} \mathbf{b}_\theta + O_p(n^{-\frac{m}{2m+d}}).
\end{aligned}$$

That is, (3.9) and the desired result are obtained. ■

Appendix B. Technical proofs in Section 4.

Proof of Theorem 4.1. From (4.2), the stationary points of PPK loss function satisfy that

$$\text{(B.1)} \quad 0 = \frac{\partial}{\partial \theta_j} \left\{ L_{PK}(\boldsymbol{\theta}) + \eta \|\hat{\delta}_{PK}^\theta\|_{L_2(\Omega)}^2 \right\}.$$

Theorem 3.4 shows the partial derivative of the PK loss function $L_{PK}(\boldsymbol{\theta})$ on $\theta_j, j = 1, \dots, q$. Next, we need to compute the partial derivative of $\|\hat{\delta}_{PK}^\theta\|_{L_2(\Omega)}^2$ on $\theta_j, j \in \{1, 2, \dots, q\}$.

$$\text{(B.2)} \quad \frac{\partial \|\hat{\delta}_{PK}^\theta\|_{L_2(\Omega)}^2}{\partial \theta_j} = \frac{\partial \int_{\Omega} (\hat{\delta}_{PK}^\theta)^2 d\mathbf{x}}{\partial \theta_j} = 2 \int_{\Omega} \hat{\delta}_{PK}^\theta \frac{\partial \hat{\delta}_{PK}^\theta}{\partial \theta_j} d\mathbf{x}.$$

where $\frac{\partial \hat{\delta}_{PK}^\theta}{\partial \theta_j}$ is shown in (A.9). Because $\int \hat{\delta}_{PK}^\theta \mathbf{g}_\theta d\mathbf{x} = \mathbf{0}$,

$$\begin{aligned}
& 2 \int_{\Omega} \hat{\delta}_{PK}^\theta \frac{\partial \hat{\delta}_{PK}^\theta}{\partial \theta_j} d\mathbf{x} = 2 \int_{\Omega} \hat{\delta}_{PK}^\theta \times \left(-\frac{\partial y^s(\mathbf{x}, \boldsymbol{\theta})}{\partial \theta_j} - \frac{\partial \mathbf{b}_\theta^T}{\partial \theta_j} \mathbf{E}_\theta^{-1} \mathbf{g}_\theta - \mathbf{b}_\theta^T \frac{\partial \mathbf{E}_\theta^{-1}}{\partial \theta_j} \mathbf{g}_\theta - \mathbf{b}_\theta^T \mathbf{E}_\theta^{-1} \frac{\partial \mathbf{g}_\theta}{\partial \theta_j} \right) d\mathbf{x}, \\
\text{(B.3)} \quad & = -2\mathbf{b}_\theta^T \mathbf{E}_\theta^{-1} \int_{\Omega} \hat{\delta}_{PK}^\theta \frac{\partial \mathbf{g}_\theta}{\partial \theta_j} d\mathbf{x}, \\
& = -2\mathbf{b}_\theta^T \mathbf{E}_\theta^{-1} \int_{\Omega} \hat{\delta}_{PK}^\theta \frac{\partial \mathbf{g}_\theta}{\partial \theta_j} d\mathbf{x} + 2\mathbf{b}_\theta^T \mathbf{E}_\theta^{-1} \int_{\Omega} \frac{\partial \mathbf{g}_\theta}{\partial \theta_j} \mathbf{g}_\theta^T d\mathbf{x} \mathbf{E}_\theta^{-1} \mathbf{b}_\theta.
\end{aligned}$$

The integration by parts formula suggests that $\frac{\partial \mathbf{b}_\theta}{\partial \theta_j} = \int_{\Omega} \hat{\delta}_{PK}^\theta \frac{\partial \mathbf{g}_\theta}{\partial \theta_j} d\mathbf{x} - \int_{\Omega} \frac{\partial y^s(\mathbf{x}, \boldsymbol{\theta})}{\partial \theta_j} \mathbf{g}_\theta d\mathbf{x}$, and $\frac{\partial \mathbf{E}_\theta}{\partial \theta_j} = 2 \int_{\Omega} \frac{\partial \mathbf{g}_\theta}{\partial \theta_j} \mathbf{g}_\theta^T d\mathbf{x}$. The derivative of inverse matrix shows that $\frac{\partial \mathbf{E}_\theta^{-1}}{\partial \theta_j} = -\mathbf{E}_\theta^{-1} \frac{\partial \mathbf{E}_\theta}{\partial \theta_j} \mathbf{E}_\theta^{-1}$. Thus we have

$$\text{(B.4)} \quad 2 \int_{\Omega} \hat{\delta}_{PK}^\theta \frac{\partial \mathbf{g}_\theta}{\partial \theta_j} d\mathbf{x} = -2\mathbf{b}_\theta^T \mathbf{E}_\theta^{-1} \frac{\partial \mathbf{b}_\theta}{\partial \theta_j} - 2\mathbf{b}_\theta^T \mathbf{E}_\theta^{-1} \int_{\Omega} \frac{\partial y^s(\mathbf{x}, \boldsymbol{\theta})}{\partial \theta_j} \mathbf{g}_\theta d\mathbf{x} - \mathbf{b}_\theta^T \frac{\partial \mathbf{E}_\theta^{-1}}{\partial \theta_j} \mathbf{b}_\theta.$$

Combining (A.13), (A.14) and (A.16), we have that (B.1) can be represented as

$$\text{(B.5)} (1 - \eta) \left[2\frac{\partial \mathbf{b}_\theta^T}{\partial \theta_j} \mathbf{E}_\theta^{-1} \mathbf{b}_\theta + \mathbf{b}_\theta^T \frac{\partial \mathbf{E}_\theta^{-1}}{\partial \theta_j} \mathbf{b}_\theta \right] - 2\eta \mathbf{b}_\theta^T \mathbf{E}_\theta^{-1} \int_{\Omega} \frac{\partial y^s(\mathbf{x}, \boldsymbol{\theta})}{\partial \theta_j} \mathbf{g}_\theta d\mathbf{x} + O_p(n^{-\frac{m}{2m+d}}).$$

Now we compare η with 1, and consider two different cases.

Case I. If $\eta = 1$, because $\mathbf{E}_\theta = \int \mathbf{g}_\theta \mathbf{g}_\theta^T d\mathbf{x}$. then we have

$$(B.6) \quad \frac{\partial}{\partial \boldsymbol{\theta}} \left\{ L_{PK}(\boldsymbol{\theta}) + \eta \|\hat{\delta}_{PK}^\theta\|_{L_2(\Omega)}^2 \right\} = -2\mathbf{b}_\theta^T + O_p(n^{-\frac{m}{2m+d}}).$$

Recall that $\boldsymbol{\theta}^s$ is a stationary point of the L_2 loss function, which satisfy that,

$$(B.7) \quad \int (\zeta(\mathbf{x}) - y^s(\mathbf{x}, \boldsymbol{\theta}^s)) \frac{\partial y^s(\mathbf{x}, \boldsymbol{\theta}^s)}{\partial \boldsymbol{\theta}} d\mathbf{x} = \mathbf{a}_{\boldsymbol{\theta}^s}^T = \mathbf{0}.$$

Because $\lim_{n \rightarrow \infty} -2\mathbf{b}_\theta^T + O_p(n^{-\frac{m}{2m+d}}) = -2\mathbf{a}_\theta^T$, we have $\boldsymbol{\theta}^s$ is a stationary point of the PPK loss function. The Hessian matrix at $\boldsymbol{\theta}^s$ can easily obtained by evaluating second derivative of the PPK loss on $\boldsymbol{\theta}$,

$$(B.8) \quad \frac{\partial^2}{\partial \boldsymbol{\theta} \partial \boldsymbol{\theta}^T} \left\{ L_{PK}(\boldsymbol{\theta}) + \eta \|\hat{\delta}_{PK}^\theta\|_{L_2(\Omega)}^2 \right\} |_{\boldsymbol{\theta}=\boldsymbol{\theta}^s} = -2 \left(\frac{\partial \mathbf{b}_\theta}{\partial \boldsymbol{\theta}} \right)^T |_{\boldsymbol{\theta}=\boldsymbol{\theta}^s} + O_p(n^{-\frac{m}{2m+d}}).$$

Moreover, Hessian matrix at $\boldsymbol{\theta}^s$ of the L_2 loss function is

$$(B.9) \quad \frac{\partial^2}{\partial \boldsymbol{\theta} \partial \boldsymbol{\theta}^T} \left\{ \|\zeta(\cdot) - y^s(\cdot, \boldsymbol{\theta})\|_{L_2(\Omega)}^2 \right\} |_{\boldsymbol{\theta}=\boldsymbol{\theta}^s} = -2 \left(\frac{\partial \mathbf{a}_\theta}{\partial \boldsymbol{\theta}} \right)^T.$$

It is easily to be proven that, $\frac{\partial \mathbf{a}_\theta}{\partial \boldsymbol{\theta}} = \lim_{n \rightarrow \infty} \frac{\partial \mathbf{b}_\theta}{\partial \boldsymbol{\theta}}$. By the order-preserving propertie of limits of real sequences, we have that if $\boldsymbol{\theta}^s$ is a local minimum (maximum) of the L_2 loss function, then $\boldsymbol{\theta}^s$ is a local minimum (maximum) of the PPK loss function.

Case II. If $\eta \neq 1$, then

$$(B.10) \quad \begin{aligned} & \frac{\partial^2}{\partial \boldsymbol{\theta} \partial \boldsymbol{\theta}^T} \left\{ L_{PK}(\boldsymbol{\theta}) + \eta \|\hat{\delta}_{PK}^\theta\|_{L_2(\Omega)}^2 \right\} |_{\boldsymbol{\theta}=\boldsymbol{\theta}^s} \\ &= (1 - \eta) \left(\frac{\partial \mathbf{b}_\theta}{\partial \boldsymbol{\theta}} \right)^T \mathbf{E}_\theta^{-1} \frac{\partial \mathbf{b}_\theta}{\partial \boldsymbol{\theta}} |_{\boldsymbol{\theta}=\boldsymbol{\theta}^s} - 2\eta \left(\frac{\partial \mathbf{b}_\theta}{\partial \boldsymbol{\theta}} \right)^T |_{\boldsymbol{\theta}=\boldsymbol{\theta}^s} + O_p(n^{-\frac{m}{2m+d}}), \\ &= (1 - \eta) \left(\frac{\partial \mathbf{b}_\theta}{\partial \boldsymbol{\theta}} \right)^T |_{\boldsymbol{\theta}=\boldsymbol{\theta}^s} \mathbf{E}_{\boldsymbol{\theta}^s}^{-1} \left\{ \frac{\partial \mathbf{b}_\theta}{\partial \boldsymbol{\theta}} - 2\eta/(1 - \eta)\mathbf{E}_\theta \right\} |_{\boldsymbol{\theta}=\boldsymbol{\theta}^s} + O_p(n^{-\frac{m}{2m+d}}), \end{aligned}$$

Now, we want to find the interval of η such that if $\frac{\partial \mathbf{b}_\theta}{\partial \boldsymbol{\theta}} |_{\boldsymbol{\theta}=\boldsymbol{\theta}^s}$ is positive (negative) definite, then $\frac{\partial^2}{\partial \boldsymbol{\theta} \partial \boldsymbol{\theta}^T} \left\{ L_{PK}(\boldsymbol{\theta}) \right\} |_{\boldsymbol{\theta}=\boldsymbol{\theta}^s}$ is negative (positive) definite. That is, the product of $(1 - \eta)$ and $\left\{ \frac{\partial \mathbf{b}_\theta}{\partial \boldsymbol{\theta}} - 2\eta/(1 - \eta)\mathbf{E}_\theta \right\} |_{\boldsymbol{\theta}=\boldsymbol{\theta}^s}$ is negative definite.

Suppose there exist constants $U \geq L$, such that

$$U\mathbf{E}_{\boldsymbol{\theta}^s} > \frac{\partial \mathbf{b}_\theta}{\partial \boldsymbol{\theta}} |_{\boldsymbol{\theta}=\boldsymbol{\theta}^s} > L\mathbf{E}_{\boldsymbol{\theta}^s}.$$

Then we have

$$(B.11) \quad \left(U - \frac{2\eta}{1 - \eta} \right) \mathbf{E}_\theta > \left\{ \frac{\partial \mathbf{b}_\theta}{\partial \boldsymbol{\theta}} - \frac{2\eta}{1 - \eta} \mathbf{E}_\theta \right\} |_{\boldsymbol{\theta}=\boldsymbol{\theta}^s} > \left(L - \frac{2\eta}{1 - \eta} \right) \mathbf{E}_\theta.$$

To evaluating the production of $1 - \eta$ and (B.11), We consider the sign of $1 - \eta$.

(A) If $(1 - \eta) > 0$, then $(U - \frac{2\eta}{1-\eta}) < 0$ is needed to guarantee that $\frac{\partial^2}{\partial\theta\partial\theta^T} \{L_{PPK}(\theta)\} |_{\theta=\theta^s}$ is negative definite. That is $U < (U + 2)\eta$ and $\eta < 1$.

(B) If $(1 - \eta) < 0$, then $(L - \frac{2\eta}{1-\eta}) > 0$ is needed. That is $L < (L + 2)\eta$ and $\eta > 1$.

By combining Case I and Case II, we have η belongs to the set $\Gamma_\lambda = \{\eta = 1\} \cup \{U < (U+2)\eta \text{ and } \eta < 1\} \cup \{L < (L+2)\eta \text{ and } \eta > 1\}$. By some easy calculations, Γ_λ can be represented as

$$(B.12) \quad \Gamma_\lambda = \begin{cases} 0 \leq \eta < \frac{L}{L+2} & L < U \leq -2 \text{ or } L = U < -2 \\ \max(0, \frac{U}{U+2}) < \eta < \frac{L}{L+2} & L < -2 < U \\ \eta > \max(0, \frac{U}{U+2}) & -2 \leq L < U \text{ or } L = U > -2 \\ \eta \geq 0 & L = U = -2 \end{cases} \quad \blacksquare$$

Proof of Theorem 4.2. First we prove the convergence of $\hat{\theta}_{PPK}$ to θ^* . The desired results can be proved by showing that

$$(B.13) \quad L_{PPK}(\theta^*) \leq \inf_{\|\theta - \theta^*\| = cn^{-\frac{m}{2m+d}}} L_{PPK}(\theta),$$

for sufficiently large n and some constant $c > 0$ to be specified later, where $\|\cdot\|$ denotes the usual Euclidean distance.

Suppose (B.13) is false. Then there exists $\tilde{\theta}$ with $\|\theta^* - \tilde{\theta}\| = cn^{-\frac{m}{2m+d}}$ so that

$$(B.14) \quad L_{PK}(\theta^*) + \eta \|\hat{\delta}_{PK}^{\theta^*}\|_{L_2(\Omega)}^2 > L_{PK}(\tilde{\theta}) + \eta \|\hat{\delta}_{PK}^{\tilde{\theta}}\|_{L_2(\Omega)}^2.$$

Because the sequence $\{\hat{\theta}_{PK}\}$ converges to θ^* in probability as n goes to infinity. By the proof of Theorem 4.2 in [17], we have that

$$(B.15) \quad L_{PK}(\theta^*) \leq \inf_{\|\theta - \theta^*\| = c_1 n^{-\frac{m}{2m+d}}} L_{PK}(\theta),$$

for sufficiently large n and some constant $c_1 > 0$. Let $c = c_1$, (B.15) implies that

$$(B.16) \quad L_{PK}(\theta^*) \leq L_{PK}(\tilde{\theta}).$$

Combining (B.14) and (B.16), we arrive at

$$(B.17) \quad \|\hat{\delta}_{PK}^{\theta^*}\|_{L_2(\Omega)}^2 > \|\hat{\delta}_{PK}^{\tilde{\theta}}\|_{L_2(\Omega)}^2.$$

On the other hand, by the definition of θ^* ,

$$(B.18) \quad \|\delta^{\theta^*}\|_{L_2(\Omega)}^2 \leq \|\delta^{\tilde{\theta}}\|_{L_2(\Omega)}^2.$$

By the uniform convergence $\hat{\delta}_{PK}^\theta$ in Theorem 3.2, we have

$$(B.19) \quad \lim_{n \rightarrow \infty} \|\hat{\delta}_{PK}^\theta\|_{L_2(\Omega)}^2 = \|\delta^\theta\|_{L_2(\Omega)}^2.$$

By the order-preserving properties of limits of real sequences, there exist $N \in \mathbf{R}$ such that, for any $n > N$,

$$(B.20) \quad \|\hat{\delta}_{PK}^{\theta^*}\|_{L_2(\Omega)}^2 \leq \|\hat{\delta}_{PK}^{\tilde{\theta}}\|_{L_2(\Omega)}^2.$$

This leads to a contradiction.

Next we prove that $\hat{\boldsymbol{\theta}}_{PPK}$ converges in distribution to a normal distribution. Denote $\hat{\delta} = \hat{\delta}_{PPK}^{\hat{\boldsymbol{\theta}}_{PPK}}$, by the definition of $\hat{\boldsymbol{\theta}}_{PPK}$, we have

$$(B.21) \quad \frac{\frac{1}{n} \sum_{i=1}^n \left(y_i - y^s(\mathbf{x}_i, \boldsymbol{\theta}) - \hat{\delta}(\mathbf{x}_i) \right)^2 + \lambda \|\hat{\delta}\|_{\mathcal{N}_{K_{\boldsymbol{\theta}}}(\Omega)}^2 + \eta \|\hat{\delta}\|_{L_2(\Omega)}^2}{\partial \boldsymbol{\theta}} \Big|_{\boldsymbol{\theta} = \hat{\boldsymbol{\theta}}_{PPK}} = 0.$$

Involved with $\frac{\partial \hat{\delta}}{\partial \theta_j} = 0, j = 1, \dots, q$, (B.21) becomes

$$(B.22) \quad \frac{\frac{1}{n} \sum_{i=1}^n \left(y_i - y^s(\mathbf{x}_i, \boldsymbol{\theta}) - \hat{\delta}(\mathbf{x}_i) \right)^2 + \lambda \|\hat{\delta}\|_{\mathcal{N}_{K_{\boldsymbol{\theta}}}(\Omega)}^2}{\partial \boldsymbol{\theta}} \Big|_{\boldsymbol{\theta} = \hat{\boldsymbol{\theta}}_{PPK}} = 0.$$

The rest part of the proof follows from the proof of Theorem 4.3 in [17]. ■

Proof of Theorem 4.3. Let $\hat{\zeta}_n(\cdot) = \hat{\delta}_{PPK}^{\hat{\boldsymbol{\theta}}_{PPK}}(\cdot) + y^s(\cdot, \hat{\boldsymbol{\theta}}_{PPK})$, which is an estimator of $\zeta(\cdot)$. The triangle inequality implies that

$$(B.23) \quad \begin{aligned} \|\hat{\zeta}_n - \zeta\|_{L_2(\Omega)} &= \|\hat{\delta}_{PPK}^{\hat{\boldsymbol{\theta}}_{PPK}} - \hat{\delta}_{PK}^{\boldsymbol{\theta}^*} + \hat{\delta}_{PK}^{\boldsymbol{\theta}^*} - \delta + y^s(\cdot, \hat{\boldsymbol{\theta}}_{PPK}) - y^s(\cdot, \boldsymbol{\theta}^*)\|_{L_2(\Omega)}, \\ &\leq \|\hat{\delta}_{PPK}^{\hat{\boldsymbol{\theta}}_{PPK}} - \hat{\delta}_{PK}^{\boldsymbol{\theta}^*}\|_{L_2(\Omega)} + \|\hat{\delta}_{PK}^{\boldsymbol{\theta}^*} - \delta\|_{L_2(\Omega)} + \\ &\quad + \|y^s(\cdot, \hat{\boldsymbol{\theta}}_{PPK}) - y^s(\cdot, \boldsymbol{\theta}^*)\|_{L_2(\Omega)}, \\ &= \text{I} + \text{II} + \text{III}. \end{aligned}$$

Next we bound (I),(II) and (III) respectively. Denote $\|\cdot\|$ as the euclidean distance.

$$(B.24) \quad \|\hat{\delta}_{PPK}^{\hat{\boldsymbol{\theta}}_{PPK}} - \hat{\delta}_{PK}^{\boldsymbol{\theta}^*}\|_{L_2(\Omega)} \leq \left\| \frac{\partial \hat{\delta}_{PK}^{\boldsymbol{\theta}}}{\partial \boldsymbol{\theta}} \Big|_{\boldsymbol{\theta}^*} \right\|_{L_2(\Omega)} \|\hat{\boldsymbol{\theta}}_{PPK} - \boldsymbol{\theta}^*\| + o_p(\|\hat{\boldsymbol{\theta}}_{PPK} - \boldsymbol{\theta}^*\|^2).$$

(A.9) suggests that

$$(B.25) \quad \frac{\partial \hat{\delta}_{PK}^{\boldsymbol{\theta}}}{\partial \theta_j} \Big|_{\boldsymbol{\theta}^*} = -\frac{\partial y^s(\mathbf{x}, \boldsymbol{\theta}^*)}{\partial \theta_j} - \frac{\partial \mathbf{b}_{\boldsymbol{\theta}^*}^T}{\partial \theta_j} \mathbf{E}_{\boldsymbol{\theta}^*}^{-1} \mathbf{g}_{\boldsymbol{\theta}^*}(\mathbf{x}) - \mathbf{b}_{\boldsymbol{\theta}^*}^T \frac{\partial \mathbf{E}_{\boldsymbol{\theta}^*}^{-1}}{\partial \theta_j} \mathbf{g}_{\boldsymbol{\theta}^*}(\mathbf{x}) - \mathbf{b}_{\boldsymbol{\theta}^*}^T \mathbf{E}_{\boldsymbol{\theta}^*}^{-1} \frac{\partial \mathbf{g}_{\boldsymbol{\theta}^*}(\mathbf{x})}{\partial \theta_j}.$$

By condition A4, $\frac{\partial \hat{\delta}_{PK}^{\boldsymbol{\theta}}}{\partial \theta_j} \Big|_{\boldsymbol{\theta}^*} < \infty$. Thus, $\left\| \frac{\partial \hat{\delta}_{PK}^{\boldsymbol{\theta}}}{\partial \theta_j} \Big|_{\boldsymbol{\theta}^*} \right\|_{L_2(\Omega)}$ can be bounded by a finite constant. Together with Theorem 4.2, we have that I = $O_p(n^{-1/2})$. Following a similar argument, we have III = $O_p(n^{-1/2})$. By using the bound in Theorem 3.2, we obtain that II = $O_p(n^{-\frac{m}{2m+d}})$. This leads to the desired result. ■

REFERENCES

- [1] M. J. BAYARRI, J. O. BERGER, R. PAULO, J. SACKS, J. A. CAFEO, J. CAVENDISH, C.-H. LIN, AND J. TU, *A framework for validation of computer models*, Technometrics, 49 (2007).
- [2] M. GU, J. PALOMO, AND J. O. BERGER, *Robustgasp: Robust gaussian stochastic process emulation in r* , arXiv preprint arXiv:1801.01874, (2018).

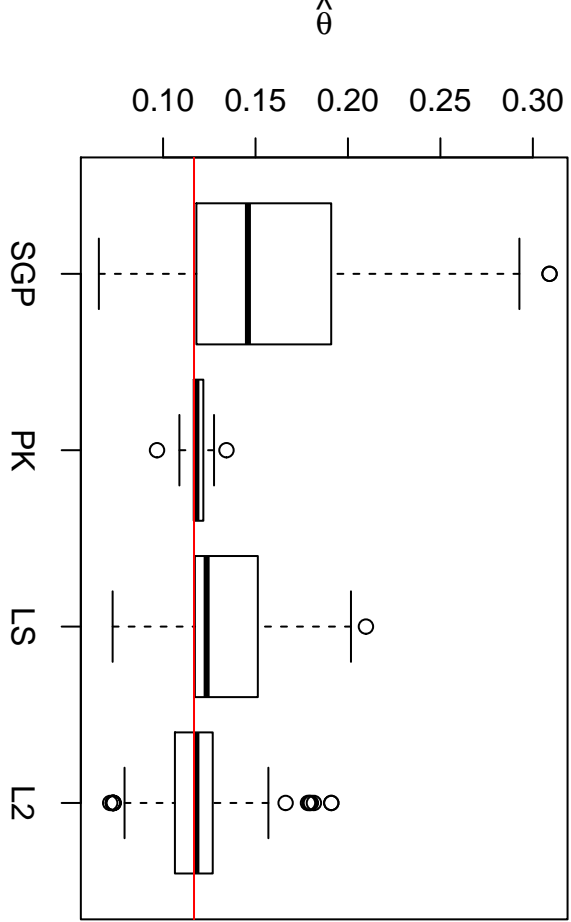
- [3] M. GU AND L. WANG, *Scaled Gaussian stochastic process for computer model calibration and prediction*, SIAM/ASA Journal on Uncertainty Quantification, 6 (2018), pp. 1555–1583.
- [4] M. GU, F. XIE, AND L. WANG, *A theoretical framework of the scaled gaussian stochastic process in prediction and calibration*, arXiv preprint arXiv:1807.03829, (2018).
- [5] G. JAMES, D. WITTEN, T. HASTIE, AND R. TIBSHIRANI, *Bias-variance trade-off for k-fold cross-validation. an introd. to stat. learn.-with appl. r*, 2013.
- [6] M. C. KENNEDY AND A. O'HAGAN, *Bayesian calibration of computer models*, Journal of the Royal Statistical Society: Series B (Statistical Methodology), 63 (2001), pp. 425–464.
- [7] M. KUHN, *A short introduction to the caret package*, R Found Stat Comput, 1 (2015).
- [8] J. S. PARK, *Tuning complex computer codes to data and optimal designs*, PhD, (1991).
- [9] M. PLUMLEE, *Bayesian calibration of inexact computer models*, Journal of the American Statistical Association, 112 (2017), pp. 1274–1285.
- [10] M. J. POWELL, *The newuoa software for unconstrained optimization without derivatives*, in Large-scale nonlinear optimization, Springer, 2006, pp. 255–297.
- [11] T. J. SANTNER, B. J. WILLIAMS, AND W. I. NOTZ, *The Design and Analysis of Computer Experiments*, Springer Science & Business Media, 2013.
- [12] B. SCHÖLKOPF, R. HERBRICH, AND A. J. SMOLA, *A generalized representer theorem*, in International Conference on Computational Learning Theory, Springer, 2001, pp. 416–426.
- [13] K. SOETAERT, *rootsolve: Nonlinear root finding, equilibrium and steady-state analysis of ordinary differential equations*, R package version, 1 (2009).
- [14] M. L. STEIN, *Interpolation of Spatial Data: Some Theory for Kriging*, Springer Science & Business Media, 1999.
- [15] J. STOER AND R. BULIRSCH, *Introduction to numerical analysis*, vol. 12, Springer Science & Business Media, 2013.
- [16] E.-G. TALBI, *Metaheuristics: from design to implementation*, vol. 74, John Wiley & Sons, 2009.
- [17] R. TUO, *Adjustments to computer models via projected kernel calibration*, SIAM/ASA Journal on Uncertainty Quantification, 7 (2019), pp. 553–578.
- [18] R. TUO, Y. WANG, AND C. WU, *On the improved rates of convergence for mat\`ern-type kernel ridge regression, with application to calibration of computer models*, SIAM/ASA Journal on Uncertainty Quantification, 8 (2020), pp. 1522–1547.
- [19] R. TUO AND C. F. J. WU, *Efficient calibration for imperfect computer models*, The Annals of Statistics, 43 (2015), pp. 2331–2352.
- [20] R. TUO AND C. F. J. WU, *A theoretical framework for calibration in computer models: parametrization, estimation and convergence properties*, SIAM/ASA Journal on Uncertainty Quantification, 4 (2016), pp. 767–795.
- [21] S. A. VAN DE GEER, *Empirical Processes in M-estimation*, vol. 6, Cambridge university press, 2000.
- [22] G. WAHBA, *Spline Models for Observational Data*, vol. 59, Siam, 1990.
- [23] Y. WANG, X. YUE, R. TUO, J. H. HUNT, AND J. SHI, *Effective model calibration via sensible variable identification and adjustment, with application to composite fuselage simulation*, Annals of Applied Statistics, 14 (2020), pp. 1759–1776.
- [24] H. WENDLAND, *Scattered Data Approximation*, vol. 17, Cambridge university press, 2004.
- [25] R. K. WONG, C. B. STORLIE, AND T. LEE, *A frequentist approach to computer model calibration*, Journal of the Royal Statistical Society: Series B (Statistical Methodology), 79 (2017), pp. 635–648.
- [26] F. XIE AND Y. XU, *Bayesian projected calibration of computer models*, Journal of the American Statistical Association, (2020), pp. 1–18.
- [27] S. XIONG, P. Z. QIAN, AND C. J. WU, *Sequential design and analysis of high-accuracy and low-accuracy computer codes*, Technometrics, 55 (2013), pp. 37–46.

This figure "calibration.jpg" is available in "jpg" format from:

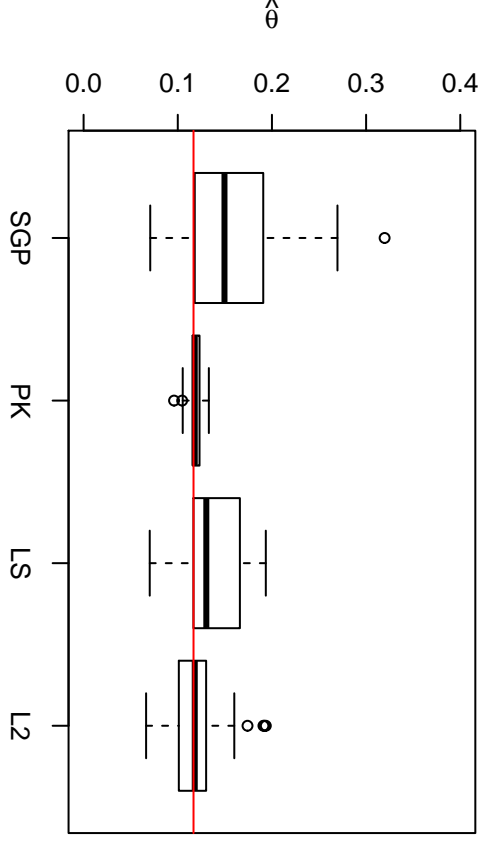
<http://arxiv.org/ps/2103.00807v1>

This figure "co.jpg" is available in "jpg" format from:

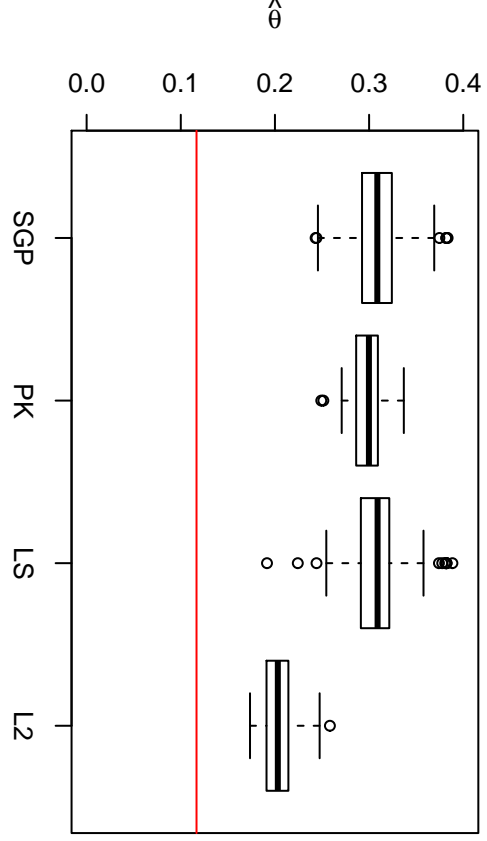
<http://arxiv.org/ps/2103.00807v1>



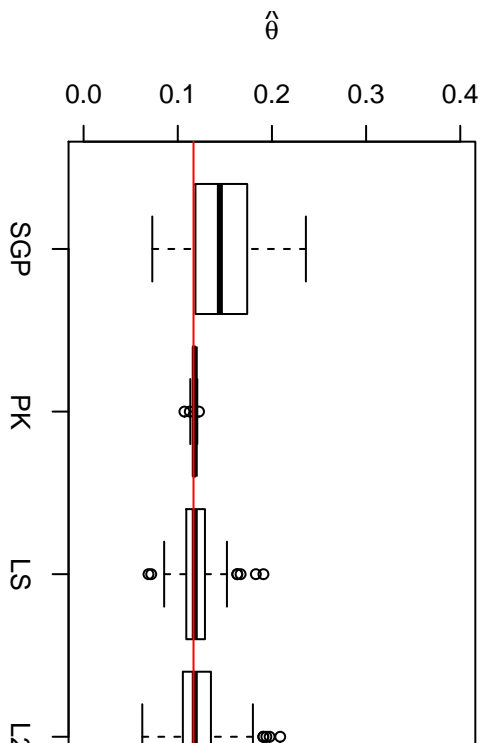
n=50



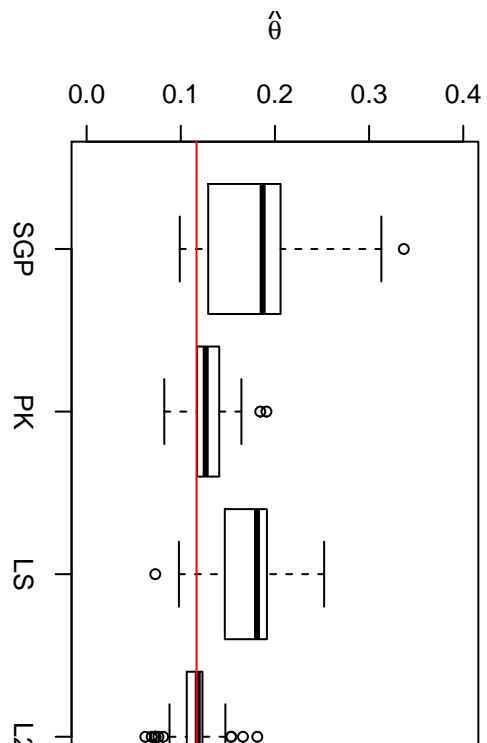
$n=50$



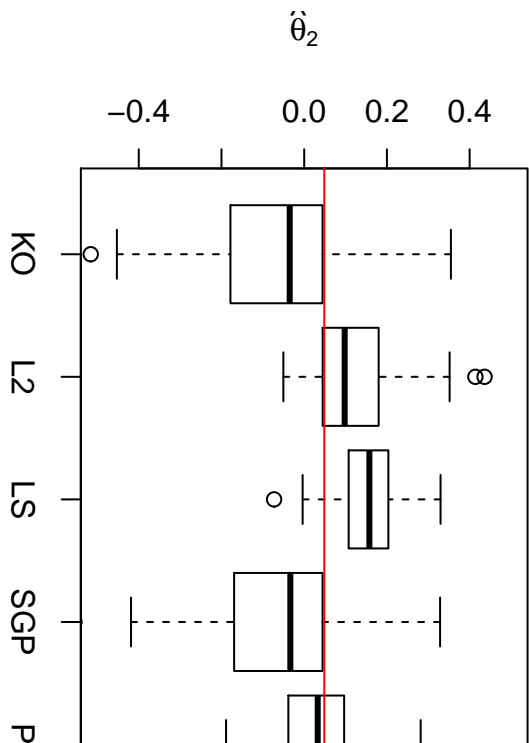
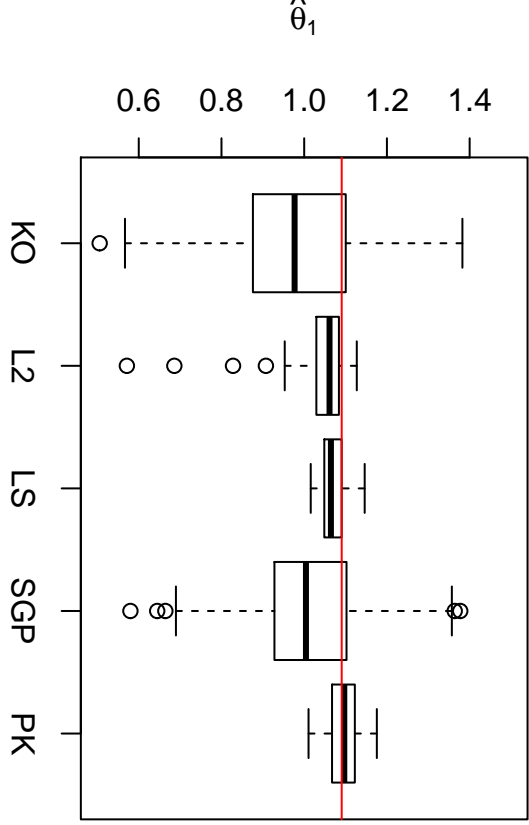
$n=6$

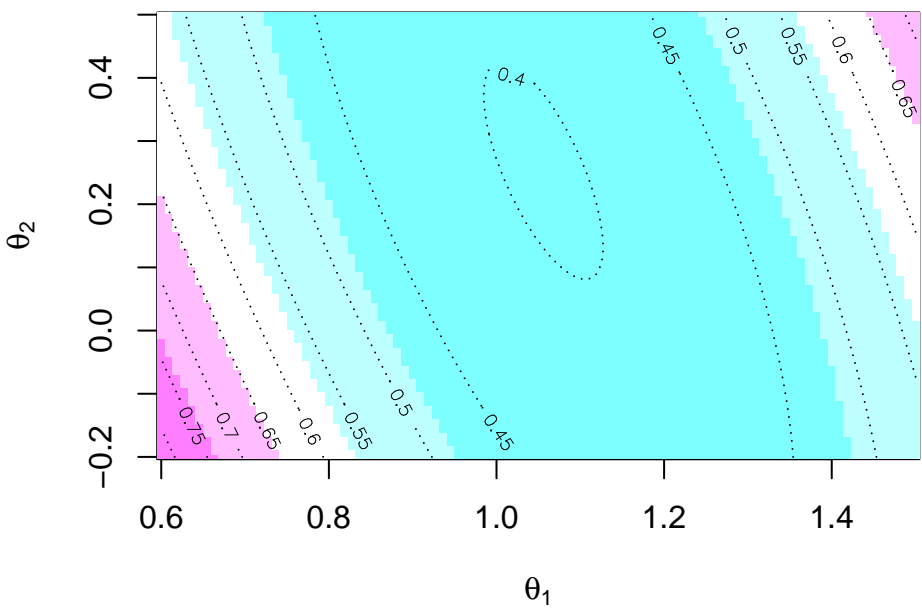


$n=100$

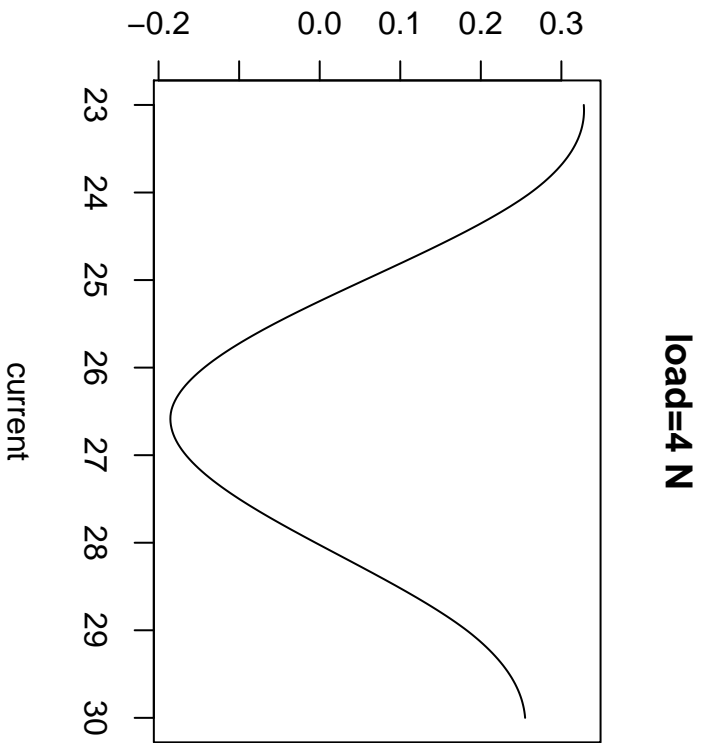


$n=20$

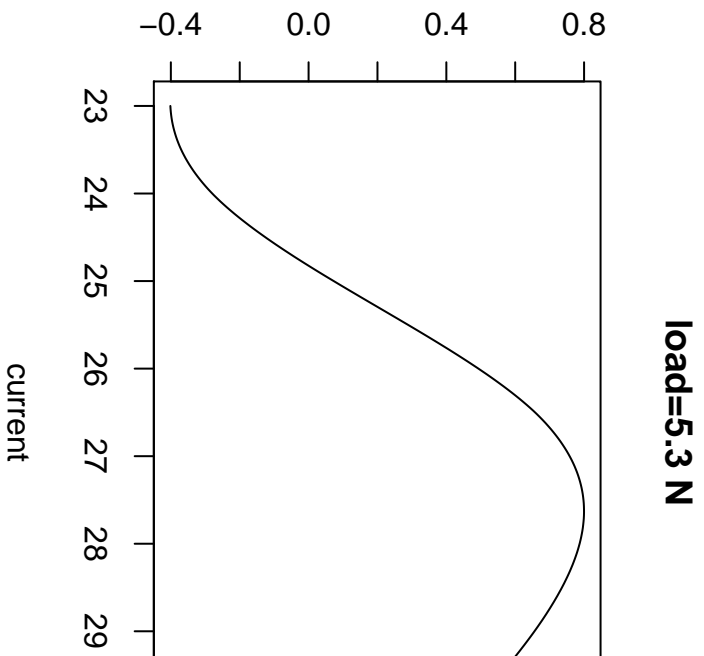




Estimation of the discrepancy function



Estimation of the discrepancy function

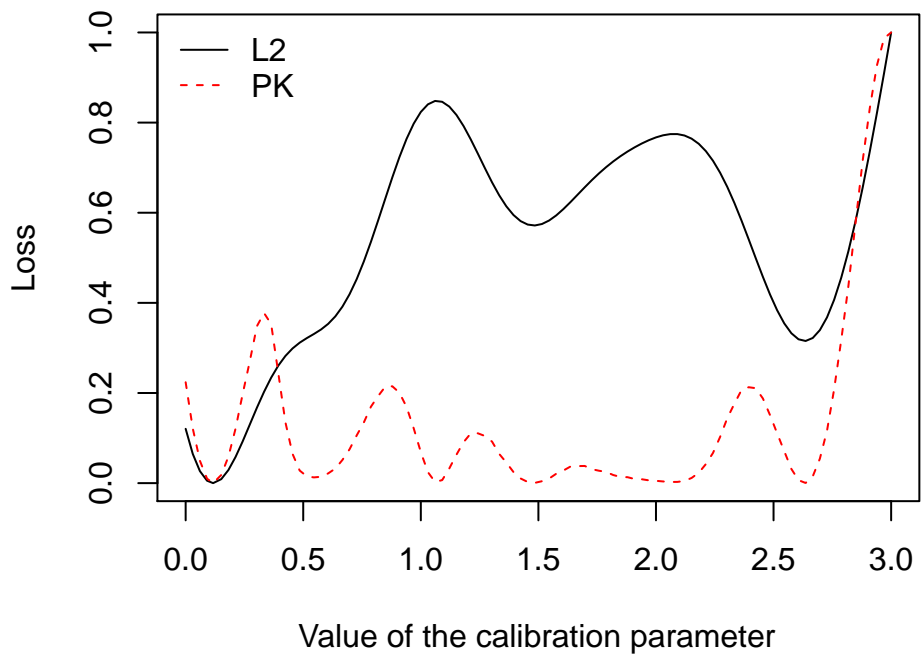


This figure "nse.jpg" is available in "jpg" format from:

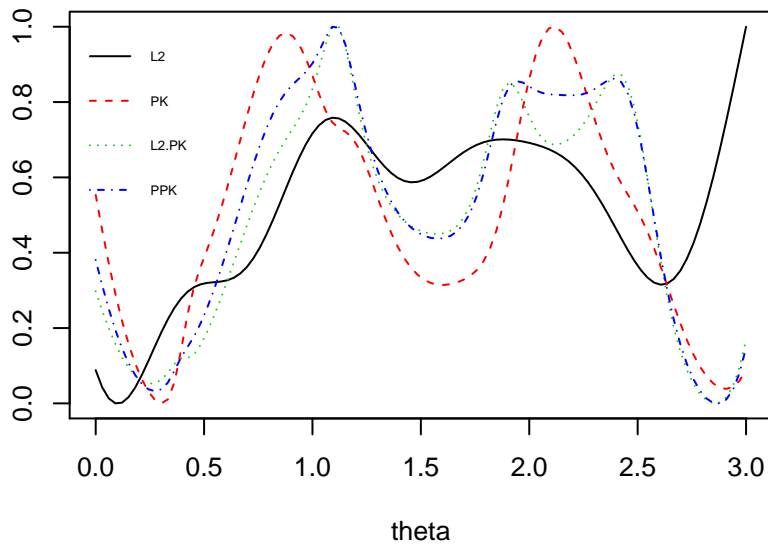
<http://arxiv.org/ps/2103.00807v1>

This figure "nve.jpg" is available in "jpg" format from:

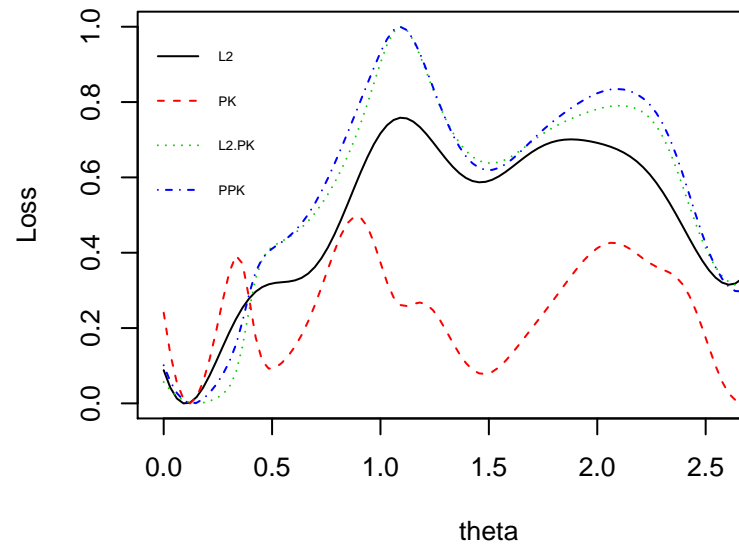
<http://arxiv.org/ps/2103.00807v1>



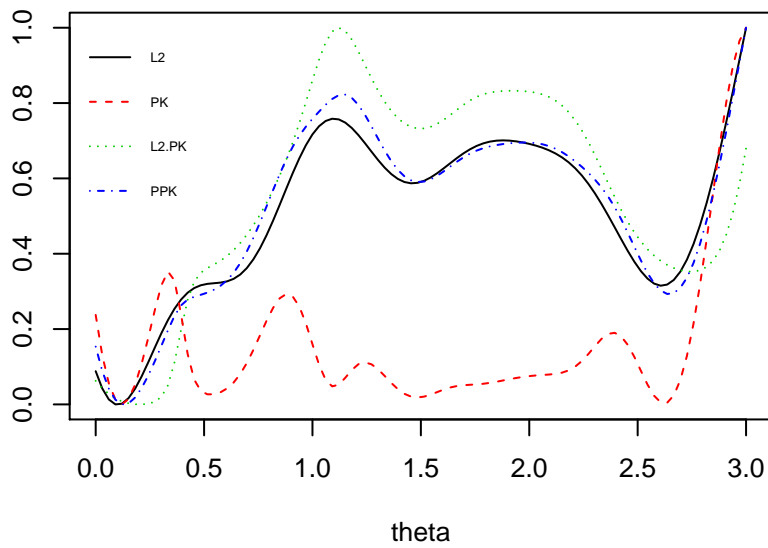
n=6



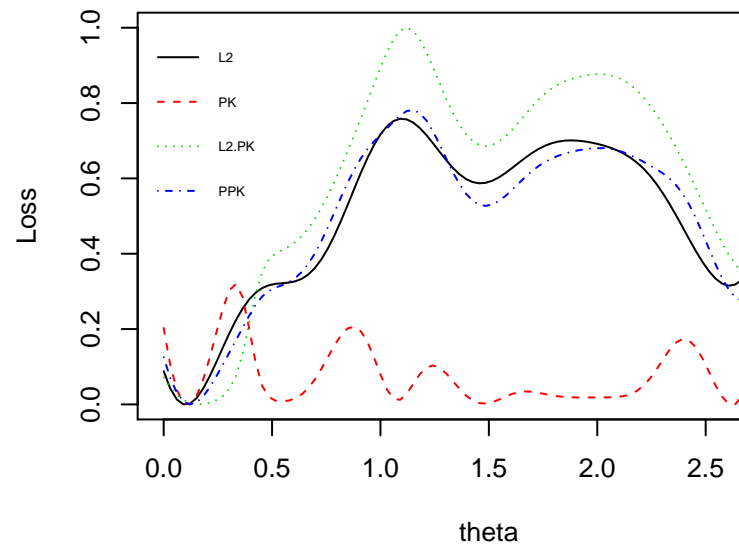
n=20



n=50



n=100



This figure "scale.jpg" is available in "jpg" format from:

<http://arxiv.org/ps/2103.00807v1>

This figure "simulator.png" is available in "png" format from:

<http://arxiv.org/ps/2103.00807v1>

This figure "spotweld.png" is available in "png" format from:

<http://arxiv.org/ps/2103.00807v1>

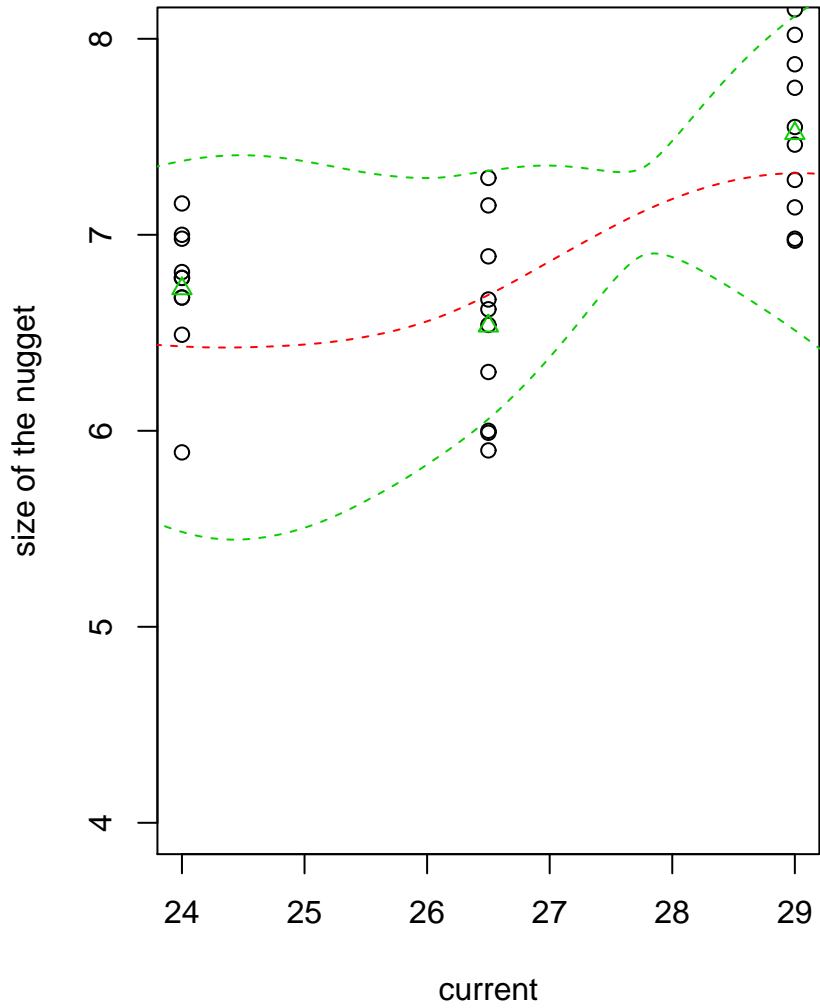
This figure "sw.jpg" is available in "jpg" format from:

<http://arxiv.org/ps/2103.00807v1>

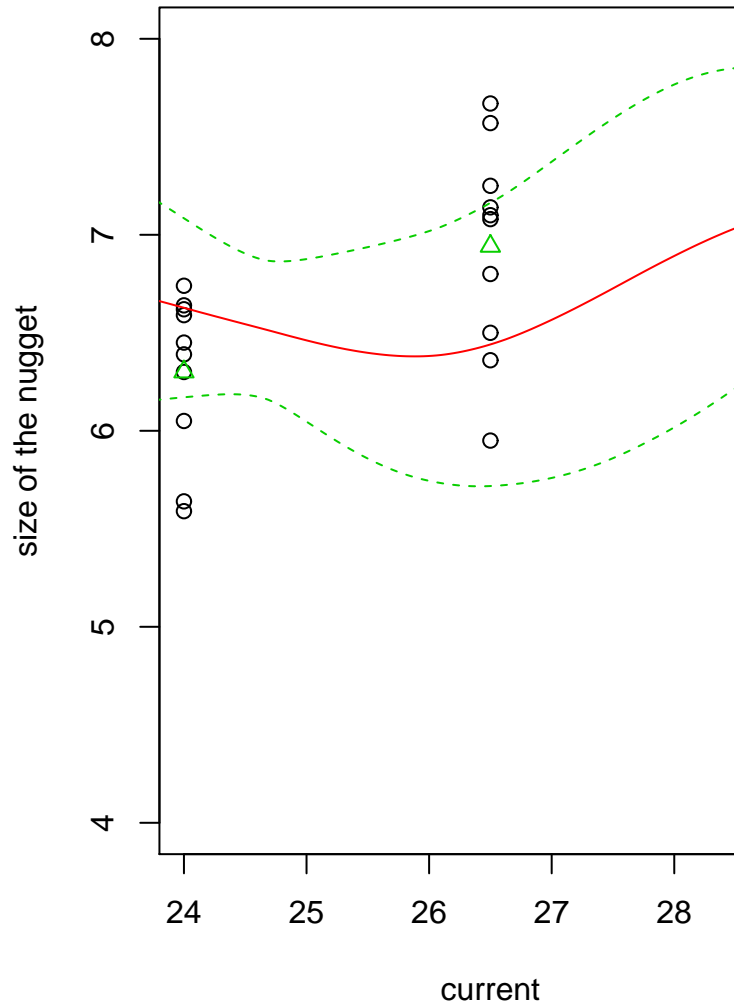
This figure "sw1.jpg" is available in "jpg" format from:

<http://arxiv.org/ps/2103.00807v1>

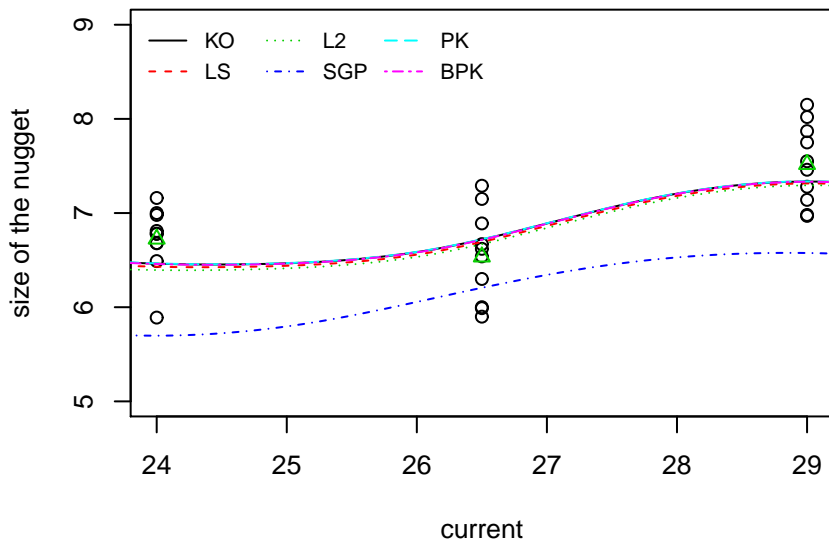
Load=4 N



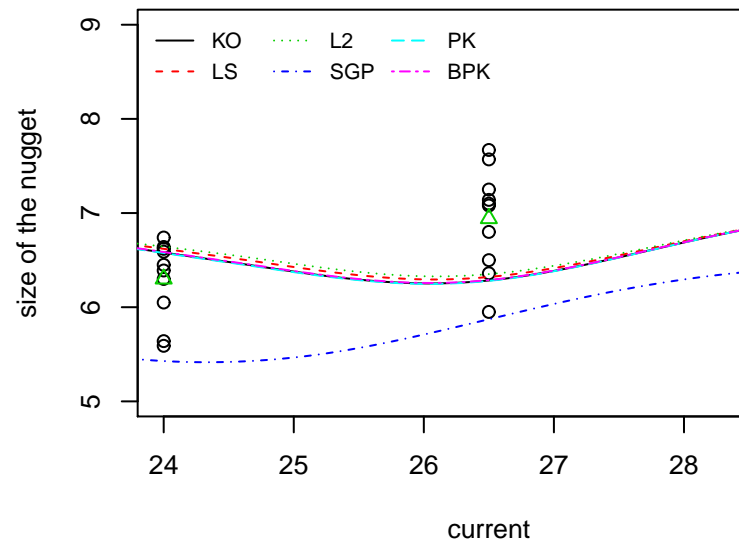
Load=5.3 N



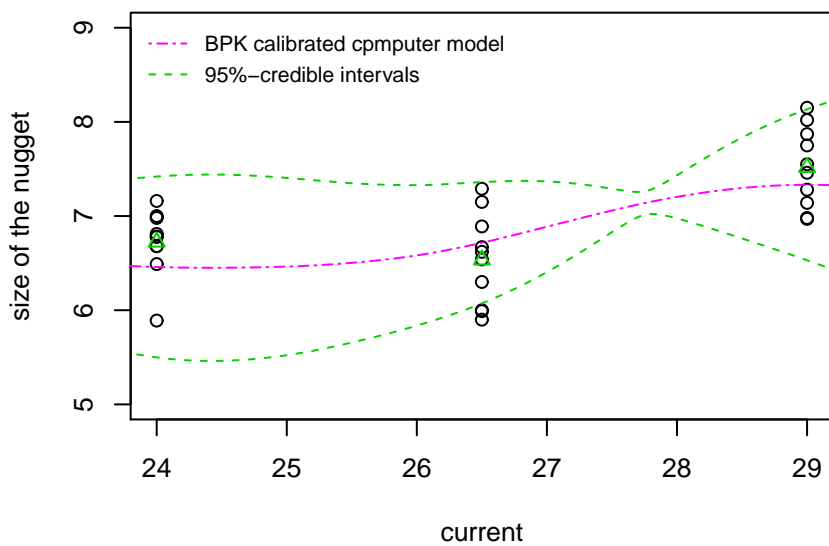
Load=4 N



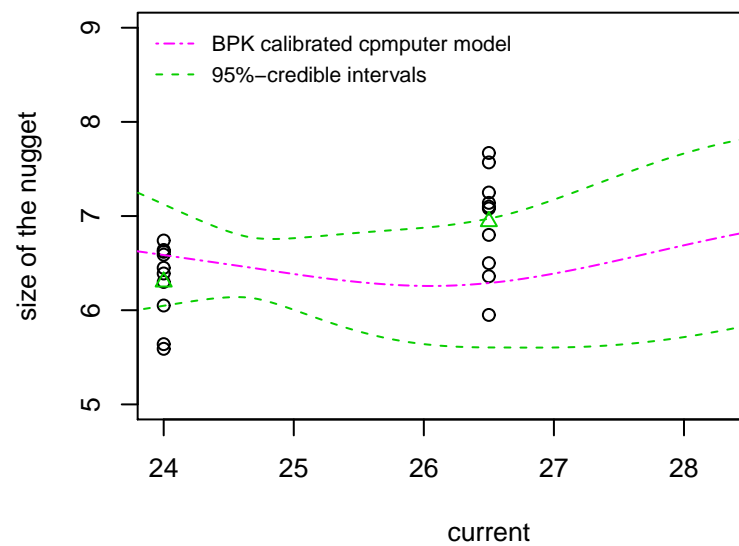
Load=5.3 N



Load=4 N



Load=5.3 N



This figure "wel.JPG" is available in "JPG" format from:

<http://arxiv.org/ps/2103.00807v1>

This figure "yosw.png" is available in "png" format from:

<http://arxiv.org/ps/2103.00807v1>

This figure "ypsw.png" is available in "png" format from:

<http://arxiv.org/ps/2103.00807v1>